UPPSALA
UNIVERSITET

Digital Comprehensive Summaries of Uppsala Dissertations from the Faculty of Science and Technology 652

First Principles Calculations of Electron Transport and Structural Damage by Intense Irradiation

CARLOS ORTIZ

ACTA
UNIVERSITATIS
UPSALIENSIS
UPPSALA
2009

ISSN 1651-6214
ISBN 978-91-554-7547-5
urn:nbn:se:uu:diva-102376

Dissertation presented at Uppsala University to be publicly examined in Polhemsalen, Lägerhyddsvägen 1, Uppsala, Friday, June 12, 2009 at 10:15 for the degree of Doctor of Philosophy. The examination will be conducted in English.

Abstract
Ortiz, C. 2009. First Principles Calculations of Electron Transport and Structural Damage by Intense Irradiation. Acta Universitatis Upsaliensis. *Digital Comprehensive Summaries of Uppsala Dissertations from the Faculty of Science and Technology* 652. 61 pp. Uppsala. ISBN 978-91-554-7547-5.

First principle electronic structure theory is used to describe the effect of crystal binding on radiation detectors, electron transport properties, and structural damage induced by intense irradiation. A large database containing general electronic structure results to which data mining algorithms can be applied in the search for new functional materials, a case study is presented for scintillator detector materials. Inelastic cross sections for the generation of secondary electron cascades through impact ionization are derived from the dielectric response of an electron gas and evolved in time with Molecular Dynamics (MD). Qualitative and quantitive estimates are presented for the excitation and relaxation of a sample irradiated with Free Electron Laser pulses. A study is presented in where the structural damage on covalent bonded crystals following intense irradiation is derived from a Tight Binding approach and evolved in time with MD in where the evolution of the sample is derived from GW theory for the quasiparticle spectra and a dedicated Boltzmann transport equation for the impact ionization.

Keywords: Condense matter theory, electronic structure, quasiparticles, GW theory, molecular dynamics, Boltzmann transport, electron transport, impact ionization, structural damage, dielectric response, structural biology, radiation detectors, scintillators, positron emission tommography

Carlos Ortiz, Materials Theory, Department of Physics and Materials Science, Box 530, Uppsala University, SE-75121 Uppsala, Sweden

ISSN 1651-6214
ISBN 978-91-554-7547-5
urn:nbn:se:uu:diva-102376 (http://urn.kb.se/resolve?urn=urn:nbn:se:uu:diva-102376)

to all bartenders...

List of Papers

This thesis is based on the following papers, which are referred to in the text by their Roman numerals.

I **Ortiz C.**, Eriksson O., Klintenberg M. *Data mining and accelerated electronic structure theory as a tool in the search for new functional materials*. *Computational Materials Science* (2009) vol. 44 (4) pp. 1042

II **Ortiz C.**, Caleman C. *Secondary Electron Cascade Dynamics in KI and CsI*. *J. Phys. Chem. C* (2007) vol. 111 (46) pp. 17442

III Caleman C., **Ortiz C.**, Marklund E., Bultmark F., Gabrysch M., Parak F.G., Hajdu J., Klintenberg M., Tîmneanu N. *Radiation damage in biological material: Electronic properties and electron impact ionization in urea*. *EPL (Europhysics Letters)* (2009) vol. 85 (1) pp. 18005

IV Caleman C., Huldt G., **Ortiz C.**, Maia F.R.N.C., Marklund E.G., Parak F.G., Hajdu J., van der Spoel D., Tîmneanu N. *Nanocrystal imaging using intense and ultrashort X-ray pulses*. Subbmitted to Proceedings of the National Academy of Sciences (PNAS).

V **Ortiz C.**, Ziaja B., Weckert E., Wang F., Jeschke H. *Radiation damage in covalent solids by intense ultra-short soft X-ray pulses*. In Manuscript

Reprints were made with permission from the publishers.

I have also contributed to the following papers, which are omitted here.

VI de Almeida J.S., Kim D.Y., **Ortiz C.**, Klintenberg M., Ahuja R. *On the dynamical stability and metallic behavior of YH_3 under pressure*. Submitted to Applied Physics Letters

VII Klintenberg M, Lebègue S., **Ortiz C.**, Sanyal B., Eriksson O. *Evolving properties of two dimensional materials, from graphene to graphite*. In manuscript. Preprint available at *arXiv:0903.2375v1*

Contents

1. Introduction

This first chapter is an attempt to introduce the reader to essential components of electronic structure theory. An outline is presented for how properties of matter can be predicted from a selection of a few physical principles. A connection is made between observable phenomena and the concept of electrons interacting in a given environment.

Matter is typically encountered in arrangements of uniform composition or *phases*. When at equilibrium, each phase is characterized by properties uniquely determined by its atomic structure, these properties can be associated to measurable quantities like density, conductivity, hardness, etc. If changes are induced to the environment, a reconfiguration of the system's equilibrium state eventually occurs. Such an event is called a *phase transition*, for example, if water is heated above its boiling temperature it restructures into a *gaseous* phase and if cooled below its freezing temperature it restructures into a *solid* phase. The purpose of technology is to take advantage of such kind of information to determine the necessary conditions for a process of interest to take place, for example, in the design of a photographic camera knowledge is required on the conditions for light to be emitted from a source, reflected from an object and then recorded by a third device. The scope of this thesis will be limited to the study of the properties in *condensed phases* of matter, which can be regarded as solids or *crystals* consisting of a very large collection of atoms under a given phase structure. The properties of such structure, including stability among others, are given by the interaction between electromagnetic charges of its constituent particles. The aim is to derive the structure of electrons in such an environment and to study the nature of the atomic bonds that follow and the conditions under which particular physical properties are realized. This is today a very profitable field of research with a wide scope of relevance, for example, in fields like radiation detection materials for medical applications, magnetic materials for data storage applications, semiconducting materials for electronic circuits, etc.

A particular phase of a material can be characterized by the relative equilibrium positions between atoms. Assuming periodicity, a smaller microscopic *unit cell* can be taken to represent a macroscopic sample. In order to derive the properties of a unit cell through computational means we need to account for the equations of motion of its charged constituents, which can be achieved by

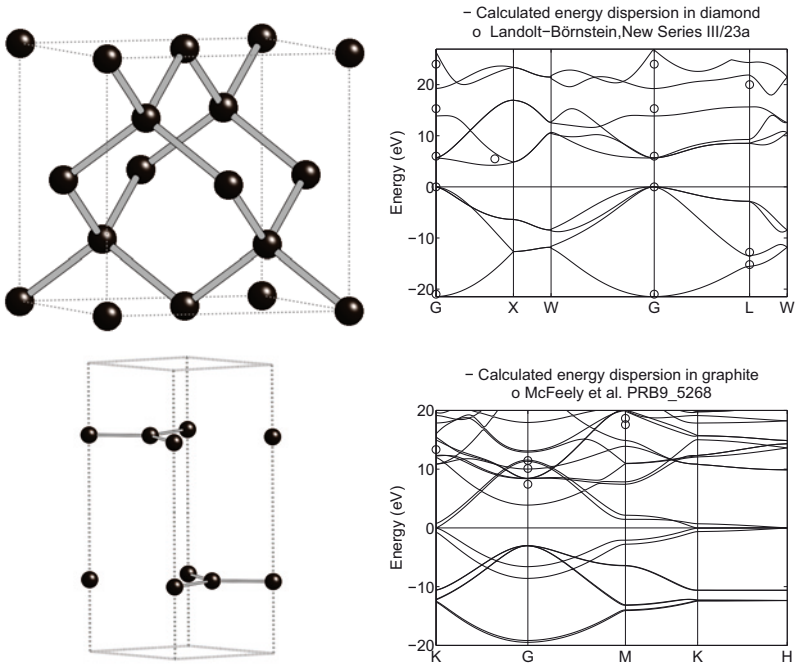

Figure 1.1: Illustration of two different unit cells of carbon (left) in its diamond (upper) and graphite (lower) phases. Carbon has atomic number, Z=6, with two of its electron in a deep energetic core state ($1s^2$ or K-shell) and four in shallow valence states ($2s^2 2p^2$). The respective symmetry operations are given by mathematical space groups $Fd\bar{3}m$ (#227) and $P6_3/mmc$ (#194) and with densities of 3.5 g cm^{-3} and 2.2 g cm^{-3}. Through the interaction of valence electrons covalent bonds are formed and characteristic electronic structures are reached. These are shown here along selected directions between high symmetry points in the unit cell (right).

exploiting symmetry relations and imposing boundary conditions. This is the way of first principle or *ab initio* methods, in where physical properties are derived using minimal information on the system under investigation together with the body of rules of physics. For example, in a comparison between two different phases of carbon, diamond and graphite, the respective electronic properties can be derived knowing only the atomic number of carbon, the dimension of the unit cell and the relative positions between atoms in it. This information is sufficient to find numerical solutions to the system of coupled equations that arises and to describe the interactions responsible for the formation of *bound states* giving each crystal its unique properties, see *Figure 1.1* for an illustration.

The description of the interaction between electromagnetic charges is taken from quantum mechanics, which is the general theory for the behavior of matter on a microscopic scale. In a free atom the allowed

solutions for the motion of the electrons, e.g. *orbitals*, are such that the electronic configuration is the most favorable energetically. When a crystal, or any general structure with a higher complexity, is formed from atomic constituents, one can think of the free atoms slowly approaching each other in space, and of electrons occupying orbitals with larger freedom of motion interacting with similar electrons of neighboring atoms. The strength of the interaction is inversely proportional to the distance, so it increases as the atoms approach, and if brought together close enough such alteration from the original environment can lead to the formation of energetically more favorable *bonding* states, and lower the total energy of the system.

In quantum mechanics, a *stationary* solution of a system is completely determined once a many-body *wavefunction*, ψ, solving the time-independent Schrödinger equation is found[1]

$$H\,\psi = E\,\psi. \tag{1.1}$$

By completely determined it is meant that, within the given theoretical framework of H, all information about the system is embedded in ψ, and knowledge of it implies that we can in principle derive, analyze and visualize any physical property. The relevant contributions to the Hamiltonian, H, can schematically be written as

$$H = T_n + T_e + V_n + V_e + V_{en}, \tag{1.2}$$

where T_n and T_e denote the kinetic contributions from the nuclei and the electrons respectively, V_n denotes the Coulomb interaction between the nuclei, V_e that of between electrons and V_{en} that between the electrons and the nucleus. Because of the high level of complexity in the Hamiltonian of real crystals[2] an exact solution to Equation (1.1) is unattainable and we need to resort to approximations. We have already introduced the notions of a perfect crystal and of a unit cell, and will resort to further approximations in the following chapter.

[1] Electrons are considered to belong to a group of elementary particles called *fermions*, obeying Fermi-Dirac statistics and of spin $\frac{1}{2}$. Although not perused here, when considering magnetic properties the spin population is relevant and either relativistic corrections need to be introduced into the Schrödinger equation or a solution to the Dirac equation is required.

[2] In diamond, for example, the number of charged constituents is of the order of 10^{24} per cm^{-3}.

2. Theoretical models

In this chapter a theoretical framework for electronic structure theory is presented. Commonly used approximations, simplifying the many-body problem of Equation (1.1) and making calculations feasible, are reviewed. For more elaborated introductions the reader is referred to references [1, 2, 3, 4, 5, 6, 7, 8, 9, 10] from which background material for this chapter has been gathered.

2.1 Approximations

2.1.1 Born-Oppenheimer approximation

Our starting point is the Hamiltonian of Equation (1.2) and we begin its modeling by making use of the Born-Oppenheimer approximation, stating that since the mass of the nucleus is much larger than the mass of the electron it can be regarded as static due to a much higher moment of inertia[1]. The kinetic contribution from the nuclei can thus be neglected, $T_n = 0$, and its electric charge regarded as a point source to a field acting on the surrounding electrons, $V_{ext} = V_n + V_{ne}$. We rewrite the Hamiltonian as

$$H = T_e + V_e + V_{ext}, \tag{2.1}$$

and the original problem is reduced to finding a solution for the motion of the electrons in a fixed background potential.

2.1.2 Independent electron approximation

It is assumed that the many-body effects of Hamiltonian can *accurately* be accounted for by introducing an effective potential, V_{eff}, which acts on each electron independently, i.e. it is assumed that the totality of electronic interactions equals the sum of all single electron interactions with V_{eff}. We write

$$V_{eff} \approx V_e + V_{ext}. \tag{2.2}$$

This approximation is valid when the electron behavior is like that of free particles, i.e. when contributions to their energy are dominated by kinetic terms and an interpretation as extended non-localized wave-like states is proper. In

[1] The mass ratio between an electron and a proton is approximatively 1:1836.

an opposite scenario, where the contributions to the electron energy in the bonding states are no longer dominated by the kinetic term and the electrons show localized behavior[2], correlation effects need to be accounted for in detail and a particle-like description is more favorable. When both localized and non-localized features are present it is particularly difficult to device a V_{eff} that remains coherent, as the electrons experience coupling at two non negligible scales simultaneously, see reference [7] for a more detailed discussion.

2.2 Bloch states and reciprocal space

The Hamiltonian reflects the symmetries of a potentially infinite but periodic crystal and is invariant to spatial displacements between equivalent positions in a unit cell, $\mathbf{R} = \sum_{i=1}^{3} n_i \hat{\mathbf{r}}_i$, where $\hat{\mathbf{r}}_i$ are the basis set vectors of the unit cell and $H(\mathbf{r}+\mathbf{R}) = H(\mathbf{r})$. Bloch's theorem states that solutions to $H(\mathbf{r})$ can be expressed in the form of a product between a periodic function carrying the periodicity of V_{eff} and a plane-wave component as

$$\psi_{\mathbf{k}}(\mathbf{r}) = u_{\mathbf{k}}(\mathbf{r}) e^{i\mathbf{k}\cdot\mathbf{r}}. \tag{2.3}$$

The index vector $\mathbf{k}$ can be shown to describe a good quantum number following from the conservation of momentum implied by the translational symmetry and satisfies $\hat{\mathbf{k}}_i \cdot \hat{\mathbf{r}}_j = 2\pi\delta_{ij}$. Furthermore, the *first Brillouin zone* (BZ) is defined as the primitive cell of the *reciprocal* lattice. An arbitrary vector in reciprocal space satisfies then the relation

$$\mathbf{k}' = \mathbf{k} + \mathbf{G}, \tag{2.4}$$

where $\mathbf{k}$ is inside BZ and $\mathbf{G}$ is a reciprocal lattice vector with $e^{i\mathbf{R}\cdot\mathbf{G}} = 1$. Following this mathematical construct, Equation (1.1) can be solved inside BZ and the results obtained are representative of the entire crystal. Assuming the wavefunctions of Equation (2.3) are reasonably smooth, the BZ can be discretized with a grid dense enough for the solutions around the neighborhood of each grid point to have small variation, and our computational task acquires thereby a finite dimension.

The different symmetry groups describing invariant operations of the relative atomic positions are available in the literature, a good example is the free-of-use database of reference [11], from which an illustration of the BZ of graphite's unit cell has been taken from and is shown here in *Figure 2.1*.

[2]Typically associated with d- and f-orbitals systems.

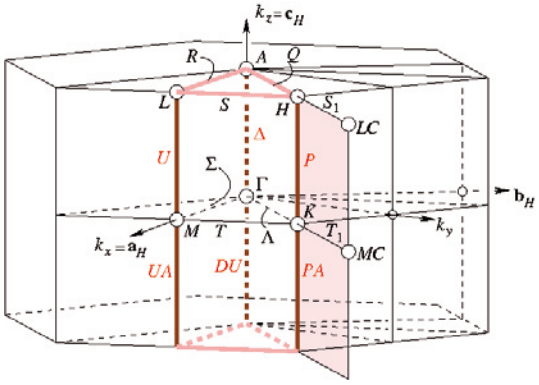

Figure 2.1: First Brillouin zone of a unit cell of graphite taken from Reference [11]. A definition of high symmetry points and directions are shown. Results for the dispersion of electronic states presented in the bottom right panel of *Figure 1.1* can be interpreted here to realize week sp^3 type of bonding. It can be seen that the K-H direction (line P) represents a vertical displacement. Small dispersion along this direction represent weak bonds, which are due to the large spacing (about 3.35 Å) between layers of carbon atoms.

2.3 Band structures

Solutions to the Hamiltonian of Equation (2.1), or rather a simplified version of it, give rise to *energy bands* or a discrete set of allowed eigenvalues for motion of the electrons, with some regions in the energy spectrum forbidden by the rules of quantum mechanics[3].

We classify among solids with respect to the band structure introducing the concepts of (i) *valence bands* being shallow energy states fully occupied by the electrons with highest energy when the system is at rest and zero temperature, (ii) *conduction bands* being the states with energies higher than those in the valence band, and (iii) the *bandgap* being the energy difference between the top of the valence band and the bottom of the conduction band, also being the minimal amount of energy required for an excitation in between these. Following the above classification three types of phases are introduced: (a) *Insulating*, where typically a large bandgap effectively blocks thermal excitations and optical transitions[4] of electrons from the valence to the conduction. (b) *Semiconducting*, where the bandgap is small enough for easy access from the valence to the conduction states through excitations. (c) *Metallic*,

[3]The distribution of eigenvalues follows the Pauli principle stating that *identical* particles (*fermions* of spin $\frac{1}{2}$) may not populate the same state simultaneously, expressed by the anti-symmetric relation $P_{ij}\psi = -\psi$ in where the operator P_{ij} permutes quantum states of electrons i and j.

[4]Photoelectric excitation of the electrons through interaction with visible light, corresponding to approximative wavelengths 300-800 nm and in an energy range of roughly 1-3 eV.

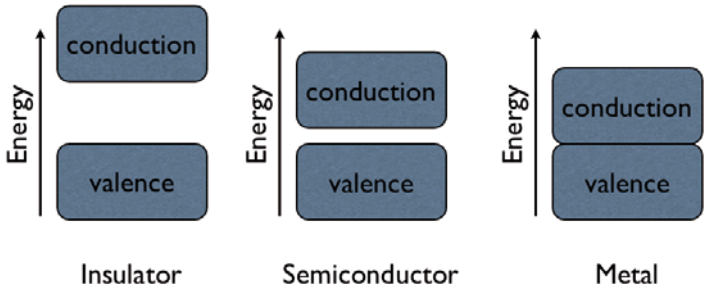

Figure 2.2: Classification of crystals with respect to the band structure. The *Fermi level* is defined as the highest energy level populated in the ground state. In the case of semiconductors, an alternative definition can be encountered in the literature in where the energy value in between the valence band maximum and the conduction band minimum is instead used.

where the valence and conduction bands overlap and thus a high electron mobility between valence and conduction states is present. See *Figure 2.2* for an illustration.

2.3.1 Exchange and correlation

The independent electron approximation assumes that the electrons in the crystal do not mutually interact in a direct manner, although in an actual system a dynamical coupling to the electron gas takes place due to the long range of the Coulomb interaction and it might lead to collective effects of the electron gas being important. A term containing these many-body interactions is high in complexity and an exact expression reproducing it remains unattainable, thus additional approximations are needed to proceed.

The Hartree model is the simplest implementation of the independent electron approximation, being a classical approach, it does not account for quantum mechanical *exchange* between identical particles. In it, the potential field V_e is assumed to be uniform and is described by the averaged field of the electric charges in the system as[5]

$$V_e \approx V_H(\mathbf{r}) = \int \frac{\rho(\mathbf{r})}{|\mathbf{r}-\mathbf{r}'|} d\mathbf{r}', \tag{2.5}$$

where $\rho(\mathbf{r})$ is the charge density of the electron gas. The corresponding N-body wavefunction is simply approximated by a product of independent

[5]Atomic units, in where normalizing constants for units of mass, m_e, length, a_0, charge, e, angular momentum, $\hbar$, energy E_h, and electrostatic force, $\frac{1}{4\pi\varepsilon_0}$, are set to unity by definition, will be used throughout this work unless explicitly stated.

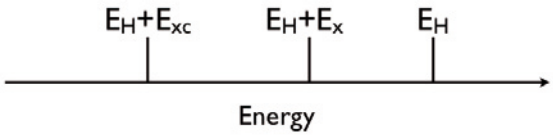

Figure 2.3: Illustration of relative values for the total energy of a system obtained at different theoretical descriptions within the independent electron approximation. The variational principle implies that the lowest energy is obtained for the most accurate description of the actual system.

solutions to one-particle Schrödinger equations, ϕ, and we write

$$\psi(\mathbf{r}_1, \mathbf{r}_2, \ldots, \mathbf{r}_N) = \phi_1(\mathbf{r}_1)\,\phi_2(\mathbf{r}_2)\cdots\phi_N(\mathbf{r}_N). \tag{2.6}$$

In the Hartree-Fock model the Pauli exclusion principle is accounted for and the wavefunction of the system is instead approximated by a Slater determinant, which corresponds to an antisymmetric product of independent one-electron solutions

$$\psi(\mathbf{r}_1, \mathbf{r}_2, \ldots, \mathbf{r}_N) = \begin{vmatrix} \phi_1(\mathbf{r}_1) & \phi_1(\mathbf{r}_2) & \ldots & \phi_1(\mathbf{r}_N) \\ \phi_2(\mathbf{r}_1) & \phi_2(\mathbf{r}_2) & \ldots & \phi_2(\mathbf{r}_N) \\ \vdots & \vdots & \ddots & \vdots \\ \phi_N(\mathbf{r}_1) & \phi_N(\mathbf{r}_2) & \ldots & \phi_N(\mathbf{r}_N) \end{vmatrix}, \tag{2.7}$$

such a product corrects the Hartree energy, E_H, with an exchange energy term, E_x, which arises as consequence of the indistinguishability between identical particles and is of statistical nature. We define the remaining discrepancy between the exact many-body and the Hartree-Fock solution to be the *correlation* of the system.

A potential, V_{xc}, accounting for both exchange and correlation of the electrons is introduced into the effective potential of Equation (2.2), generating a correction term to the total energy, E_{xc}. As implied by the variational principle and by the fact that a more accurate description of the system is employed, E_{xc} lowers the total energy of the system, see *Figure 2.3* for an illustration. We write

$$V_e = V_H + V_{xc}, \tag{2.8}$$

and regard the Hartree-Fock correction to the Hartree approximation as the *first* term in an expansion series of V_{xc}, see Section 2.5 for a further discussion on the remaining terms of such an expansion.

2.4 Density functional theory

In references [12, 13], it was shown that for an arbitrary electronic system under the influence of a static external potential, $V_{ext}(\mathbf{r})$, its ground-state energy could be written as a functional of the density

$$E[\rho(\mathbf{r})] \equiv \int V_{ext}(\mathbf{r})\rho(\mathbf{r})\,d\mathbf{r} + F[\rho(\mathbf{r})], \tag{2.9}$$

where the term, $F[\rho(\mathbf{r})]$, is regarded as universal in the sense that it does not depend on $V_{ext}(\mathbf{r})$ and thus remains the same for all systems. The contributions to this functional can, as previously, be divided into kinetic and potential terms, and $F[\rho(\mathbf{r})]$ rewritten into a sum between a non-interacting kinetic contribution, T_s, a classical Hartree term, E_H, and a many-body exchange-correlation term, E_{xc}. These are defined as

$$\begin{aligned}
T_s[\rho(\mathbf{r})] &\equiv \frac{1}{2}\int \nabla_{\mathbf{r}}\nabla_{\mathbf{r}'}\rho(\mathbf{r},\mathbf{r}')\big|_{\mathbf{r}=\mathbf{r}'}\,d\mathbf{r} \\
E_H[\rho(\mathbf{r})] &\equiv \frac{1}{2}\iint \frac{\rho(\mathbf{r})\rho(\mathbf{r}')}{|\mathbf{r}-\mathbf{r}'|}d\mathbf{r}d\mathbf{r}' \\
E_{xc}[\rho(\mathbf{r})] &\equiv \frac{1}{2}\iint \frac{C_2(\mathbf{r},\mathbf{r}')}{|\mathbf{r}-\mathbf{r}'|}d\mathbf{r}d\mathbf{r}'.
\end{aligned}$$

The density matrix above is given by $\rho(\mathbf{r},\mathbf{r}') = \langle\psi(\mathbf{r})|\psi(\mathbf{r}')\rangle$ and the one-particle density by $\rho(\mathbf{r}) = \rho(\mathbf{r},\mathbf{r})$. The two-particle statistical function

$$C_2(\mathbf{r}_i,\mathbf{r}_j) \equiv \rho(\mathbf{r}_i)\rho(\mathbf{r}_j)\left[n_{xc}(\mathbf{r}_i,\mathbf{r}_j) - 1\right], \tag{2.10}$$

includes the *exchange-correlation hole*, $n_{xc}(\mathbf{r}_i,\mathbf{r}_j)$, which represents the reduced probability of finding electron i in the charge distribution of electron j. This formalism is consistent with the previous statement that the exchange-correlation contribution lowers the total energy of the system (see *Figure 2.3*). It was also shown that $V_{ext}(\mathbf{r})$ is uniquely determined by the ground state charge density, $\rho_0(\mathbf{r})$, implying that the energy minimum of the system is given by a density profile associated with $V_{ext}(\mathbf{r})$ and its information about the system in the ground state expressible as a functional relation to $V_{ext}[\rho_0(\mathbf{r})]$.

In combination with the variational principle, Equation (2.9) leads to the Kohn-Sham system of equations [14],

$$\left[T_s + V_{eff}(\mathbf{r})\right]\phi_i = E_i\phi_i \tag{2.11}$$

$$V_{eff}(\mathbf{r}) = V_H(\mathbf{r}) + V_{xc}(\mathbf{r}) + V_{ext}(\mathbf{r}). \tag{2.12}$$

After a solution of these has been found, an updated density profile can be constructed by performing a sum over all independent one-particle solutions

$$\rho(\mathbf{r}) = \sum_{i=1}^{N} |\phi_i(\mathbf{r}_i)|^2. \tag{2.13}$$

Following an iteration of Equations (2.11-2.13), a new set of Kohn-Sham equations can be constructed with the updated density profile and a new solutions obtained, progressively lowering the systems total energy because of the variational principle. This iterative procedure can be repeated until a *convergence* criterium is reached, for example, a requirement on a given minimal discrepancy between solutions from two subsequent iterations.

Electronic densities are far from uniform in many crystals, and no expressions for an universal $E_{xc}[\rho(\mathbf{r})]$ are available. Over the years the main concern in DFT has been how to make the most accurate and economic description of such term for an arbitrary system. Many models are available in the literature and we restrict the discussion regarding the ground state to treat only the simplest approach.

2.4.1 Local density approximation

For systems with small variations on the density profile, a self consistent scheme to solve Equations (2.11-2.13) known as the Local Density Approximation (LDA) was introduced [13]. In it, an expression for the exchange-correlation functional was given as

$$E_{xc}[\rho(\mathbf{r})] \approx \int \rho(\mathbf{r})\varepsilon_{xc}[\rho(\mathbf{r})]\, d\mathbf{r}, \tag{2.14}$$

with ε_{xc} being the one-electron exchange-correlaton energy for a *homogenous* electron distribution. Within the limits of validity of the LDA, the exchange part of ε_{xc} can be calculated analytically and the correlation part estimated and parametrized with the aid of Quantum Monte-Carlo calculations [15, 16].

DFT remains an exact ground state theory until an approximative relation for $E_{xc}[\rho(\mathbf{r})]$ like that of Equation (2.14) is introduced, after which solutions cease to describe proper electronic states and become instead artificial objects that yield the correct ground state density, but lack a clear physical interpretation[6]. The success of the LDA in terms of its accuracy and wide range of applicability was unanticipated [18] and it has in retrospective been argued that it is partly due to the fulfillment of a sum rule which correctly expresses the normalization of the exchange-correlation hole [19].

[6]With the exception of the uppermost occupied orbital whose interpretation as an exact ionization potential was shown in [17]

2.5 Self-energy

Further analysis of the electron gas beyond the ground state requires an account of the *electrodynamic response* to the crystal potential following perturbations from the equilibrium by processes like single particle excitation, or *band transitions*, and collective excitations of the electron gas through *plasmons*[7], see references [5, 6, 20, 21, 22] for a more general discussion. The many-body effects of the exchange-correlation term are in their totality expressed by the self-energy of the electrons, Σ, or the sum of all possible electronic *events*. Σ is a complex quantity with a real and an imaginary part and can be derived by Green's functions in Feynman diagram techniques. The imaginary part of Σ results from the fact that the states being described are not proper eigenstates of the system, instead, these so called *quasiparticles* describe an excited state that can relax through transfer of energy and momentum to the electron gas. The relaxation rate, or inverse lifetime, for these real collisions is responsible for the imaginary contribution and is given by Γ= -2 Im Σ, while the real part is due to virtual collisions [22]. In this section an account will be given for how to obtain an expression for Σ from techniques of electronic structure theory outlined in previous sections.

2.5.1 Green's functions

The one-particle Green's function is formally defined as an expectation value

$$G(x,x') = -i\,\langle\Psi|\,T\left[c(x)c^{\dagger}(x')\right]|\Psi\rangle\,, \tag{2.15}$$

where $|\Psi\rangle$ is the ground state many-electron function, $c(x)$ and $c^{\dagger}(x)$ respective creation and annihilation operators of a quantum state x, and T the time order operator. The above relation can be interpreted as a probability amplitude for the propagation of an electron, or an electron hole, from a point x, in a coordinate system that gathers all relevant quantum numbers, to a different point x'. In such a framework $G(x,x')$ becomes the the information carrying variable as was the wavefunction in Equation (1.1). A non-interacting one-particle Green's function, $G^0(x,x')$, can be constructed under the free electron approximation from ground state solutions to the Schrödinger equation of Section 2.4. $G(x,x')$ can then be obtained through the *Dyson equation*

$$G(x,x') = G_0(x,x') + G_0(x,x')\Sigma G(x,x'). \tag{2.16}$$

[7] Plasmons are quantum states in where the long range contributions of the Coulomb interaction result in the collective excitation of plasma resonances.

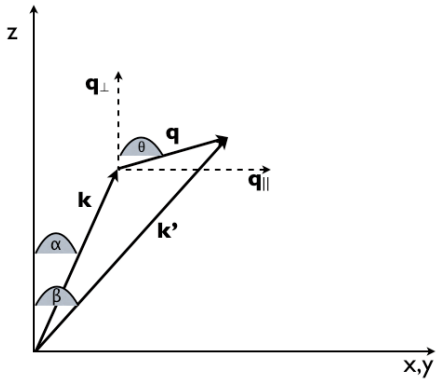

Figure 2.4: Illustration of an inelastic electronic process with momentum transfer corresponding to the wavevector $\mathbf{q} = \mathbf{k}' - \mathbf{k}$.

2.5.2 Dielectric properties, screening and the Random Phase Approximation

Following the excitation of an electron from the ground state, the sudden change in occupation of eigenstates can be interpreted as a positive charge, or an *electron hole*, being present in the system at a given position. The remaining electrons will respond to such perturbation and become attracted to the charge imbalance, thus effectively reducing or *screening* it.

The allowed single-particle transitions between eigenstates of the electron gas in a given electronic structure are expressed by the dielectric function, $\varepsilon(\mathbf{q},\omega)$, where an *inelastic* electronic process yielding a transfer of momentum and of energy, $\hbar\mathbf{q}$ and $\hbar\omega$, respectively, is described, see *Figure 2.4* for an illustration. The event likelihood and corresponding perturbation to the crystal potential are in turn characterized by $\varepsilon(\mathbf{q},\omega)$, which, assuming a linear response and making use of first order perturbation theory together with *dipole* selection rules for the allowed transitions, can be expressed as [6, 20, 23, 24]

$$\varepsilon(\mathbf{q},\omega) = 1 - \lim_{\eta\to 0}\frac{4\pi e^2}{q^2}\sum_{\mathbf{k}\in BZ}\sum_{v\in VB}\sum_{c\in CB}\frac{|\langle c,\mathbf{k}+\mathbf{q}|\, e^{i\mathbf{q}\cdot\mathbf{r}}\,|v,\mathbf{k}\rangle|}{E_{\mathbf{k}+\mathbf{q}} - E_{\mathbf{k}} - \hbar\omega + i\hbar\eta}, \qquad (2.17)$$

in where *BZ*, *VB* and *CB* denote the first Brillouin zone, valence and conduction bands, respectively. Local field effects to $\varepsilon(\mathbf{q},\omega)$ are described in detail in references [25, 26].

The imaginary part of $\varepsilon(\mathbf{q},\omega)^{-1}$ can be compared directly to photoabsorption measurements (where $\mathbf{q}$=0). At larger energy transfers, direct optical transitions described in terms of first-order perturbation theory occur much stronger than indirect optical transitions described by second-order perturbations. Furthermore, $\varepsilon(\mathbf{q},\omega)$ satisfies a set of sum rules [27, 28]. In particular,

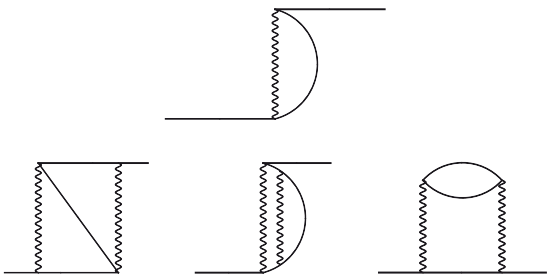

Figure 2.5: The exchange diagram contains a single Coulomb line (up), correlation diagrams contain two or more Coulomb lines, three configurations containing exactly two Coulomb lines are possible (down).

when **q**=0 a relation usually referred to as the "f-sum rule" is given by

$$\omega_p^2 = -\frac{2}{\pi}\int_0^\infty \omega \,\mathrm{Im}\,\varepsilon(0,\omega)^{-1}\,d\omega, \tag{2.18}$$

where the plasma frequency, ω_p, is given by

$$\omega_p^2 = \frac{4\pi\aleph e^2}{m_e}, \tag{2.19}$$

and $\aleph$ is the number of electrons per unit volume in the medium. Through sum rule analyses $\varepsilon(\mathbf{q},\omega)$ becomes a measure of the number of particles available for inelastic transitions of $\hbar\mathbf{q}$ and $\hbar\omega$.

In a perturbative approach, the electron self-energy is given by the sum of an infinite number of *ordered* contributions, where the order of the interaction can be expressed by the number of Coulomb lines in a corresponding Feynman diagram. In this framework, the exchange term from the Hartree-Fock approximation is equivalent to the contribution from a Feynman diagram containing one single Coloumb line. The correlation term amounts to the remaining higher order diagrams containing more than one Coulomb line, see *Figure 2.5* for an illustration.

The Random Phase Approximation (RPA) [6, 20, 21, 23, 29] assumes that phase factors in a collective description of the electron gas average out, since the contributing terms depend on the position of neighboring particles in the electron gas and a random distribution of delocalized states is assumed. In Feynman framework, the RPA can be shown to retain contributions from all possible closed fermion loops as in the lower rightmost diagram of *Figure 2.5*. The summation gives rise to an infinite series, of which the first terms are illustrated in *Figure 2.6*, that converges to what is called the RPA *polarization*, $P(\mathbf{q},\omega)$, and relates to the changes in the charge density originating in changes

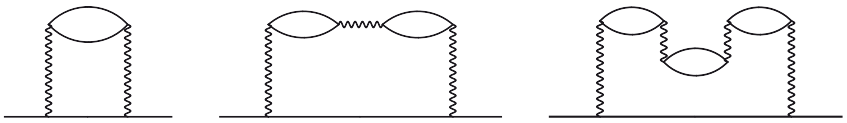

Figure 2.6: The Random Phase Approximation retains only contributions from closed fermion loops, which can be interpreted as virtual creation and annihilation of a particle-hole pair.

to the crystal field. $\varepsilon(\mathbf{q},\omega)$ can be expressed in terms of $P(\mathbf{q},\omega)$ as

$$\varepsilon(\mathbf{q},\omega) = 1 - V(\mathbf{q})P(\mathbf{q},\omega), \tag{2.20}$$

with $V(\mathbf{q}) = \frac{4\pi e^2}{q^2}$ a bare coulomb term for the many-body interaction.

Within the RPA, $P(\mathbf{q},\omega)$ accounts for uncorrelated electron-hole effects, failing to describe excitonic effects but accounting for a good description of the collective plasma oscillation, or plasmons, under high electronic polarizability [30]. The screened interaction potential, $W(\mathbf{q})$, is defined as

$$W(\mathbf{q}) = \varepsilon^{-1}(\mathbf{q},\omega)V(\mathbf{q}). \tag{2.21}$$

For a further discussion regarding the RPA, we refer the reader to reference [21] where the conditions for its validity are discussed and to reference [6] for a discussion on higher order contributions.

2.5.3 GW approximation

In electronic structure theory, the GW approximation to the self energy [31], or GW theory, substitutes the bare Coulomb potential of the Hartree-Fock approximation, V_H, with a dynamically screened potential, W, that accounts for charge fluctuations following polarization of the electron gas through the incorporation of the RPA dielectric response of the system by an induced one-particle perturbation to the electric field. Within this framework, one obtains estimates for quasiparticle energies describing the conduction band structure of the crystal on a more sound theoretical basis than from ground state theories such as DFT.

The self-energy is given by a set of coupled integral equations known as Hedin's equations

$$\Sigma = iGW\Gamma \tag{2.22}$$

$$W = V_H + WPV_H \tag{2.23}$$

$$P = -iGG\Gamma, \tag{2.24}$$

where G is a one-particle Green's function. Γ is called the *vertex function* and is given by $\Gamma = 1 + \frac{\delta\Sigma}{\delta G} GG\Gamma$. The GW Approximation consist of setting $\Gamma = 1$ and thus obtaining

$$\Sigma = iGW \tag{2.25}$$

$$P = -iGG. \tag{2.26}$$

The self-energy is expressed as a product on the screened interaction, W, rather than the long-ranged Coulomb potential, V_H. If the screening effects of correlation are neglected, only the term $\Sigma = iGV = V_x$ is retained, which amounts to the Hartree-Fock exchange term of Section (2.3.1). The GW approximation overcomes many of the shortcomings of the models of DFT and yields bandgaps in better agreement with experiment [32]. At sufficiently low temperatures where strong collective effects can be neglected, GW quasiparticles can be taken to give a complete description of the spectra from excited states in direct and inverse photoemission experiments [9, 33]. The quasiparticle energies, E^{qp}, are obtained from the relation

$$H_H\Psi(x) + \int dx' \, \Sigma(x,x')\Psi(x') = E^{qp}\Psi(x), \tag{2.27}$$

where H_H is includes kinetic and Hartree terms previously discussed.

2.6 Free electron limit and collective excitations

When studying transport or mobility properties of the electrons following irradiation, there are two different energy regimes to consider. In one, the available eigenstates are distinctly dispersive, meaning that there is a significant curvature to the energy bands with respect to reciprocal space (see *Figure 1.1*), hence a signature of such structure is observed and a detailed quantum mechanical treatment for the allowed transitions is necessary in the analysis. In another, higher in energy, the allowed eigenstates approach a continuum in where the non-dispersive free electron relation $E = \hbar^2\mathbf{k}^2/2m$ holds, such a regime is entered typically when energies larger than 50-100 eV from the valence band maximum are being considered.

A free electron like material is one in which the optical loss function shows a predominant peak due to well-defined plasmons, which have an energy close to the free electron value for ω_p defined in Equation (2.19). If excited, plasmons describe almost completely the long range part of the Coulomb interaction and constitute an independent mode of elementary oscillations. In a one-electron-like excitation picture, in where collective responses to the polarizability are expected to be fast and give rise to a short effective screening

in the electron gas, the remaining elementary excitations are of an essentially independent electron character [5, 30].

2.7 Probing matter with light

In probing the structure of matter, useful experimental information can be extracted from a *kinematical* analysis following exposure to light pulses. Different light sources are characterized by the radiation's wavelength, intensity, brightness, temporal and spatial distribution, repetition rate and coherence properties. As photons interact with the sample, energy can be deposited into the system and electrons excited to higher energies. An accurate description of the properties of an excited state as well as an understanding of the dominating relaxation mechanisms are crucial to technological applications.

When the number of excited states is moderate or the *carrier density* is low, the relaxation mechanisms of an excited state are attainable within the framework of condensed matter physics. As the carrier density increases a non-equilibrium state is approached in where, eventually, the collective behavior of the electron gas dominates. Following intense irradiation, a significant fraction of the electrons might become excited from the ground state and the population of plasma states, from lower to higher temperatures, can be reached in a controlled manner. The energy scales in where condensed matter effects are relevant ranges from hard X-rays ($\sim$keV), in where the core electrons may be excited and ejected from the sample through the photoelectric effect and where the coherent scattering of photons may be used for structural determination through the recording of a diffraction pattern, to the optical regime ($\sim$eV), where transitions between the valence bands to the conduction bands and the excitation of plasmons may be promoted and electron transport properties of the material investigated.

The stabilizing forces of the lattice structure, expressible by a potential energy surface (PES), can drastically alter due to the repopulation of energy levels. Thermodynamically, energy dissipation in an excited sample is mediated through an adiabatic coupling between the electrons and the lattice vibrations, or *phonons*, and occurs on a longer timescale than that of the lifetime of an excited electronic state (roughly picoseconds vs. femtoseconds). Phase transitions follow as the PES is softened by the excitations and the stabilizing forces of the lattice structure no longer can counterbalance the atomic motion. Experimental data on non-adiabatic phase transitions is scarce and a complete understanding on the nature of the atomic motion in such states remains unclear. Time resolved diffraction measurements, recorded through *pump-probe* techniques where a pump laser is used to excite the sample and a probe pulse

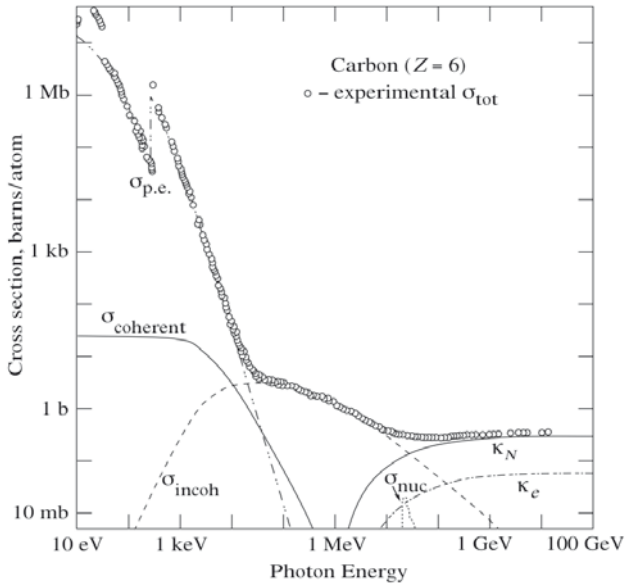

Figure 2.7: Photon total cross section as a function of energy taken from reference [34]. Photoelectric absorption, $\sigma_{p.e}$, in where the photon energy is transfered to an electron is seen to be the dominant contribution below 10 keV. The coherent scattering of photons, $\sigma_{coherent}$, is useful in diffraction experiments, from which the irradiated sample's structure can be determined. The above relations may also be obtained from the extensive NIST database available at `http://physics.nist.gov/PhysRefData/`. It is also shown here that the incoherent or Compton scattering, σ_{incoh}, for energies larger than 1 keV and thus a non-negligeble energy loss mechanism.

used to record information on the excited state, provide an excellent tool to obtain dynamical structural information on such transitions.

2.7.1 Kinematics

A photon traveling in a condensed medium can interact either elastically, in where no change on the scatterer's internal structure occurs, or inelastically, in where an energy transfer takes place and a change in the scatterer's internal quantum state is induced. The kinematic relations, or probabilities for a given outcome of a collision, are usually expressed in terms of cross sections. Photon scattering by the nuclei and pair production occur at energy scales beyond the scope of this thesis and will be neglected, see *Figure 2.7* for an illustration of processes contributing to carbons total photon cross section. For hard X-rays, the photon energy exceeds by far the energies of binding orbitals and interference effects from different scattering centers are small,

thus the total elastic cross section is well represented by a convolution of atomic cross sections of respective atoms in the crystal. See reference [35] for a tabulation of photon scattering cross section for elements $Z \leq 100$.

Through its passage through a medium a maximum penetration depth is eventually reached due to scattering, a mean value of this depth is referred to as the *attenuation length*, furthermore, incoherent scattering is referred to as *Compton scattering* in the literature. Direct excitation of electrons in the crystal are mediated mainly through the photoelectric effect, in where a photon is absorbed by the medium and its energy transfered to an electron[8]. As the excited state evolves in the crystal it relaxes, or experiences recombinations towards the ground state through a sequence of transitions being either *radiative*, in where the energy transfer between two states is mediated through the emission of a photon at a characteristic energy, or *non-radiative*, in where the energetic state transfers energy and momentum to the crystal and the excitation of *secondary electrons* to less energetic states might be promoted. Emitted photons and electrons that acquire energies above the ionization threshold of the sample can be recorded directly and carry a signature of the band structure. In the event of favorable sample geometries and in combination with an efficient extraction potential being applied, the less energetic secondary electrons may also be extracted and recorded by a detector. The ratio between the total number of extracted electrons with respect to the number absorbed photons is referred to in the literature as the electron *yield*. Following the excitation of a core electron a non-radiative relaxation process of particular importance for technological applications follows, in where a bound electron recombines with the hole created and the excitation of a second electron is promoted, this three-body process is called *Auger* recombination. Estimates on the recombination rates of such processes are attainable from first principles, see for example references [36, 37].

Electron–photon kinematics is widely used in technological applications, one example is that of light emitting diodes in where high *quantum efficiency*, being the ratio between the number of radiative recombinations to the total number of recombinations of excited electrons, is employed. At high carrier concentrations, the quantum efficiency is limited by non-radiative loss mechanisms, a phenomenon commonly referred to as *efficiency droop*. The precise nature of these loss has been the subject of intense debate, and a variety of candidates has been discussed. Experimentally, the discrimination between competing non-radiative processes poses a problem as individual signatures

[8] Photons are *bosons* of spin 1, carrying neither mass nor electric charge. Since spin is a quantity conserved in the transition, the energy transfer must be such that the absorbed photon excites an electron to an energy state differing in orbital momentum by ± 1. Furthermore, excitations from the K-shell core electrons of lighter elements are predominant for hard X-rays.

can not be observed. Auger recombination has been proposed as the dominant source of the efficiency droop at high carrier concentrations, scaling with the cubic power of the carrier concentration [38].

2.7.2 Free Electron Lasers

New light sources have had a significant influence on natural sciences throughout history. Currently, we are witnessing the advent of a new generation of light sources, combining the strength of high fluency in synchrotron radiation with coherence properties of lasers. Expectations on these X-ray Free Electron Laser (XFEL) sources are high, as they are expected to provide ultra-short and extremely intense coherent X-ray pulses with a peak brilliance exceeding that of conventional synchrotron sources by more than eight orders of magnitude, see *Figure 2.8* for an illustration. The FLASH soft XFEL in

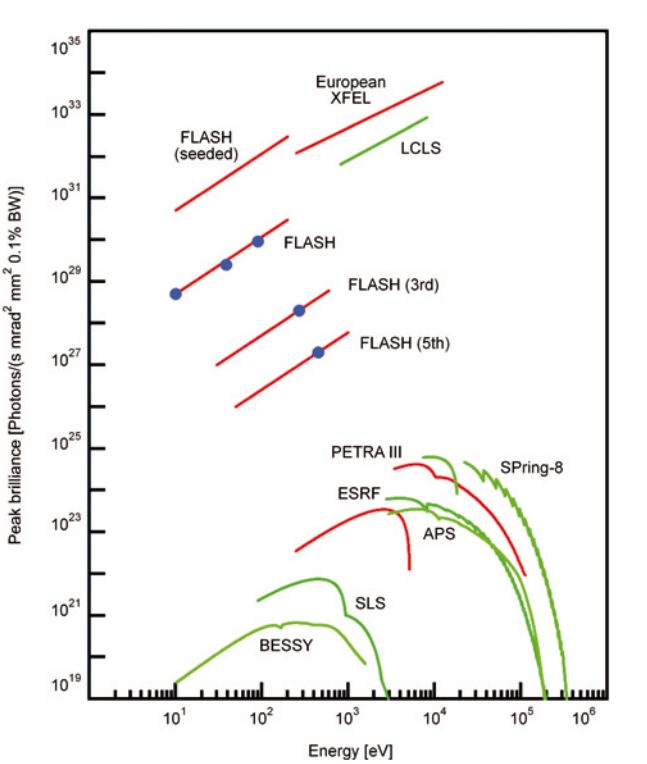

Figure 2.8: Expected peak brilliance and photon energy range of femtosecond XFEL sources.

Germany [39] was the first to reach into the X-ray frequencies, and it is a fully operational user facility today. The LINAC Coherent Light Source (LCLS) [40] in the USA is a hard X-ray laser expected to provide user beam

later this year. Similar projects are under way in Japan [41] and in Europe [42].

As a consequence, a large effort is being made by the scientific community to explore the nature of interactions of intense XFELs with matter. Short, intense, coherent, hard X-ray pulses can be exploited for new experiments in disciplines ranging from experimental astrophysics to structural biology [43] and could make single molecule imaging, i.e. retrieving atomic structures from large biological molecules without the need of a crystalline sample, feasible [44, 45].

A sample exposed to intense hard XFEL pulses will be ionized extensively, which leads to structural damage and eventual destruction of the sample. The time scale on which this process occurs is critical for obtaining an interpretable diffraction pattern to yield an atomic structure of the sample. In principle, the X-ray pulse must be short enough such that the entire pulse passes through the sample before a major reconfiguration of the atomic and electronic configurations takes place. The ionizations due to photoabsorbption and subsequent secondary processes affect the ability to get useful structural information from the diffraction pattern in three ways. (i) Ionization decreases the elastic X-ray scattering power of the atoms. (ii) Removal of electrons from the atoms leaves behind positively charged ions that repel each other due to Coulomb forces, leading to the destruction of the structure. (iii) Free electrons either leave the sample, if their energy is high enough, or remain in the sample as an excited background electron gas, in which case they will contribute to noise in the diffraction pattern.

Recent advances in femtosecond X-ray diffraction techniques have lead to a deepened understanding of light-matter interaction at ultra-short time scales, and of charge transport properties at high carrier densities. The insight to be gained from these near-future-experiments carries promises of a diverse class of new technological applications. Radiation emitted from XFELs is delivered in pulses of a few tens to several hundred femtoseconds length. Their unique properties will enable for probing dynamic states of matter resolving transitions and reactions in a system with femtosecond temporal resolution, and with wide-ranging implications to solid state physics, material science, chemistry, and biology. In particular, the accurate understanding and description of temporal characteristics of radiation damage is necessary in order to estimate the range of pulse lengths at which imaging with XFELs would be possible. And even though it will be crucial to the success of the imaging experiments, understanding the interaction of intense XFEL pulses with atomic systems and the underlying dynamics is still in its infancy, see for example refferences [46, 47, 48, 49].

2.8 Electron transport theory

Electromagnetically charged particles couple through photons. In a condensed medium and at non-relativistic energies, the propagation of a charged particle couples either to the dielectric response, ε, in the case of an electric charge, or to the to the permeability, μ, in the case of a magnetic charge[9]. In the following, an account is given for how to derive the scattering properties of a charged electron traveling in a condensed medium, omitting magnetic transport properties.

2.8.1 Electron elastic scattering

In the event of elastic scattering of an electron by the Coulomb potential of a crystal, the elastic cross section can be determined directly from solutions of the wave equation to the system by means of a partial wave approach, in where the angular dependence of the differential cross section is expressed in terms of a scattering amplitude which is dependent on a direction k and on an angle θ variable [1, 50]

$$\frac{d\sigma}{dkd\theta} = |f(k,\theta)|^2, \tag{2.28}$$

and given by a superposition of partial waves describing the scattering medium as

$$f(k,\theta) = \sum_{l=0}^{\infty} (2l+1) a_l(k) P_l(\cos\theta), \tag{2.29}$$

in where $P_l(\cos\theta)$ are the Legendre polynomials and $a_l(k)$ partial wave amplitudes,

$$a_l(k) = \frac{1}{2ik}\left[e^{2i\delta_l(k)} - 1\right], \tag{2.30}$$

given by the *phase shift* relation,

$$\tan\delta_l(k) = -k\int_0^{\infty} j_l(kr) V(r) R_l(k,r) r^2\, dr, \tag{2.31}$$

in where $j_l(kr)$ are spherical Bessel functions and and $R_l(k,r)$ radial solutions to the scattering potential $V(r)$.

[9] In vacuum, the speed of light is given by the relation $c = \frac{1}{\sqrt{\varepsilon_0\mu_0}}$, which also illustrates a relationship between the propagation of electromagnetic radiation to the conductivity properties of the medium.

2.8.2 Electron inelastic scattering from first principles

Inelastic collisions may be treated in two different regimes with respect to the scattering particles velocity relative to the mean orbital velocity of an electron in a given state, one fast and one slow regime. In condensed phases both the total and the differential cross sections are significant, the latter for soft collisions in particular, as relative variations over a narrow energy range need to be modeled accurately. The first description of the *stopping power* of materials for fast particles was first given by Bohr [51], and a quantum mechanical theory was first formulated by Bethe [52] and extended to condensed materials by Fano [53], see reference [8] for a historical review.

Electrons loose energy mainly due to excitation or ionization of the medium in where the loss rates scale logarithmically with energy. The probability per unit time, τ, for an inelastic process of losses $\hbar\mathbf{q}$ and $\hbar\omega$ to occur is given by [24]

$$\tau(\mathbf{q},\omega) = \frac{8\pi e^2}{q^2}\omega \ \mathrm{Im}\ \varepsilon(\mathbf{q},\omega)^{-1}. \tag{2.32}$$

In a free-electron gas[10] , the inelastic scattering of an electron passing through the medium is represented through the electron density, ρ, characterized by the average distance between electrons, r_s, given by

$$r_s = \sqrt[3]{\frac{3\pi\rho}{4}}. \tag{2.33}$$

In the interpretation of an excited electron's passage through a medium, the Inelastic Mean Free Path (IMFP), λ_{in}, or average distance travelled between scattering events, is an useful quantity. At an energy, E_k, it is given by the relation [6]

$$\lambda_{in}(E_k) = \frac{k\hbar^2}{2m_e|\mathrm{Im}\ \Sigma(E_k)|}. \tag{2.34}$$

Neglecting exchange and correlation, assuming an isotropic medium, and in systems of free-electron gas behavior Im $\Sigma(k)$ can be expressed by [22]

$$\mathrm{Im}\ \Sigma(E_k) = -\frac{e^2}{2\pi^2}\int\frac{d^3q}{q^2}\int_0^{E_k} d\omega\ \mathrm{Im}\ \frac{1}{\varepsilon(q,\omega)}, \tag{2.35}$$

In a homogenous and isotropic medium ($q = |\mathbf{q}|$) and given $\varepsilon(q,\omega)$, the probability of an energy loss $\hbar\omega$ per unit distance travelled by an electron carrying an energy E is given by the Differential Inverse Mean Free Path (DIMFP) [54]

[10] Whenever assuming a free-electron gas relation for the energy dispersion effects of the electronic structure are neglected, these are significant typically at an energy range below 100 eV.

$$\tau(E,\omega) = \frac{1}{\pi E}\int_{q_-}^{q_+}\frac{dq}{q}\mathrm{Im}\left[-\varepsilon(q,\omega)^{-1}\right], \tag{2.36}$$

in where the relation $\hbar q_{\pm} = \sqrt{2m_e}(\sqrt{E} \pm \sqrt{E-\hbar\omega})$ sets the limits for the allowed momentum transfer. Furthermore, λ_{in}, is given by

$$\lambda_{in}^{-1}(E) = \int d\omega\, \tau(E,\omega). \tag{2.37}$$

For many materials detailed knowledge of $\varepsilon(\mathbf{q},\omega)$ is often either absent in the literature, or the available experimental information limited to a narrow energy range associated with large uncertainties due to difficulties in their experimental recording.

In the limit $\mathbf{q} = 0$, a model by Powell and Penn uses information of the dielectric function at the optical limit, $\varepsilon(0,\omega)$, to derive $\lambda_{in}(k)$, introducing a pseudo-charge density r_s^p that ensures [55, 56].

$$\mathrm{Im}\ \varepsilon^{-1}(0,\omega) = -\frac{\pi}{2}\omega_p(r_s^p)\delta(\omega-\omega_p(r_s^p)), \tag{2.38}$$

where $\omega_p(r_s^p)$ is the plasma frequency of Equation (2.19), thus satisfying the f-sum rule. The above approximation has been used extensively in the literature for derivations of λ_{in}, and is commonly known as the TPP model, see references [57, 58, 59]. An alternative model by Ashley [60] assumes a simple quadratic connection between anergy and momentum and models $\varepsilon(q,\omega)$ as

$$\mathrm{Im}\ \varepsilon^{-1}(q,\omega) = \int_0^{\infty} d\omega' \frac{\omega'}{\omega}\mathrm{Im}\ \varepsilon^{-1}(0,\omega')\,\delta\left(\omega-\left(\omega'+\frac{q^2}{2}\right)\right). \tag{2.39}$$

2.8.3 Binary encounter model for electron transport

Mott's collision theory [61] describes the interaction between two free electrons, generalizing the Rutherford cross section through the inclusion of exchange and gives an accurate account of hard collisions. Soft collisions are mediated mainly trough the dipole interaction between the incident particle and the medium [52]. Mott's approach is the starting point of the Binary Encounter Dipole model (BED) [62], incorporating a term describing the *differential dipole oscillation strength* given by

$$\frac{df}{d\omega} = -\omega\frac{2}{\omega_p^2}\mathrm{Im}\ \varepsilon^{-1}(\mathbf{q},\omega). \tag{2.40}$$

The BED model provides a recipe to construct ionization cross sections accounting for the discretized structure of eigenvalues in a cumulative manner, and can be used for any target atom or molecule as long as the

corresponding $\frac{df}{d\omega}$ is known. These can be obtained from either theoretical or experimental photoionization cross sections. A simplified version of the BED, the Binary Encounter Bethe model (BEB), was proposed simultaneously for when $\frac{df}{d\omega}$ is unavailable.

The orbital structure is in total described by variables B, U and N representing binding energy, average kinetic energy and occupation number respectively, and the divergence of the Mott cross section in the limits of energy loss, W→0 or W→T, in electron–electron collisions, where T is the available energy carried by the impact electron, is resolved by replacing the kinetic energy of the excited electron, W, by the energy transfer variable, E=W+B. An expression for the binary encounter cross section reads

$$\begin{aligned}\frac{\sigma_{BE}(E,T)}{dE} =& \frac{4\pi a_0 RN}{T+U+B}\left\{\frac{1}{E^2}-\frac{1}{E(T-W)}\right.\\ &\left.+\frac{1}{(T-W)^2}+\frac{4U}{3}\left[\frac{1}{E^3}+\frac{1}{(T-W)^3}\right]\right\}.\end{aligned} \tag{2.41}$$

when expressing the above energy variables in units of B as

$$\begin{aligned} t &= T/B \\ \omega &= W/B \\ u &= U/B \\ S &= \frac{4\pi a_0 R^2 N}{B^2}, \end{aligned} \tag{2.42}$$

Equation (2.41) can be expressed in a more compact form

$$\frac{d\sigma_{BE}(\omega,t)}{d\omega} = \frac{S}{B}\sum_{n=1}^{3} F_n(t)\left[f_n(\omega)+f_n(t-\omega)\right], \tag{2.43}$$

where

$$\begin{aligned} F_1 &= -\frac{F_2}{t+1} \\ F_2 &= \frac{1}{t+u+1} \\ F_3 &= \frac{4u}{3(t+u+1)}, \end{aligned} \tag{2.44}$$

and

$$\begin{aligned} f_n(\omega) &= (\omega+1)^{-n} \\ f_n(t-\omega) &= (t-\omega)^{-n}. \end{aligned} \tag{2.45}$$

The n=1 term represents interference between the primary and secondary electrons, the n=2 arises from close collisions, and the n=3 term accounts for momentum distribution of a bound electron being ionized. Terms containing $f_n(\omega)$ represent secondary electrons ejected from the target during the collision, while the terms containing $f_n(t-\omega)$ describe the scattered primary electrons which have lost energy. In the low energy transfer limit, $\omega \ll$ t, the $f_n(t-\omega)$ terms may be ignored and the n=3 terms are identified through Bethe asymptotics yielding

$$\begin{aligned} F_3 &= \frac{\ln t}{t} \\ f_3(\omega) &= \frac{1}{N(\omega+1)} \frac{df(\omega)}{d\omega}. \end{aligned} \tag{2.46}$$

Although the BED model is substantially simpler to use than most first principle theories for electron impact ionization, in cases when nothing is known about $\frac{df}{d\omega}$ the BEB model can be used ionization cross sections of correct orders of magnitude, in where $f_3(w)$ is given by Equation (2.45) and

$$\begin{aligned} F_3 &= \frac{Q \ln t}{t+u+1} \\ Q &= 2f_3. \end{aligned} \tag{2.47}$$

2.8.4 Electron–hole pair production

Kane [63, 64, 65] presented a first derivation for the rate of inelastic scattering of electrons by considering the production of electron–hole pairs in silicon. Henke et al. [66] performed further investigations for semiconductors and insulators as compared to gold, both theoretically and experimentally, with respect to the electron yield and energy distribution, accounting for both electron and phonon scattering, but under a free-electron band description and thus not fully treating the bound nature of the collective excitations. Strong structural features for the alkali halide SE energy distributions and suggested these to arise from single-electron promotions from the valence band due to plasmon de-excitations.

Fraser [67, 68] examined the total yield and pulsed quantum efficiency with respect to photon incidence angle and energy, and presented a model describing the dynamics in terms of averaged parameters for the SE creation energy and their inelastic mean free path. Akkerman et al. [69, 70, 71, 72, 73, 74] introduced a model in which a more rigorous treatment of the electron–phonon scattering was implemented for CsI, but obtained an energy spread for the SE deviating from Henke's experiments. This discrepancy was claimed to arise from the lack of treatment of plasmons in their model [75].

3. Computational methods

Regarding the motion of each electron in a crystalline solid as of in a static periodic potential field paved the way for theoretical treatment and calculation of properties derived from the crystal band structure. The early calculations agreed only semi-quantitatively with the experimental results. This led to the development of semi-empirical techniques in where introduced parameters were adjusted so that calculations would generate results that accurately fit the experimental findings, see reference [76] for a historical review. In this chapter, it will be assumed that the required information regarding the structure of the crystal can be obtained from databases available in the literature, see for example reference [77], and a review of the computational techniques used to produce the results presented in this thesis will be given.

3.1 Basis set, self consistency and convergence

The periodic potential in which the motion of the electron takes place has the following features: Near each nucleus, due to small distances, it approaches the corresponding atomic potential and the electron behaves as if in an isolated atomic environment and in a spherically symmetric manner. In between the atoms, due to a larger distance, the potential varies much less rapidly. A smooth transition is required in between these two regions. In its entirety, the potential is often assumed to be spherically symmetric within spheres surrounding the atoms and constant outside. Continuous wavefunctions are expanded in spherical harmonics and radial solutions of the wave equation within the spheres, and in plane waves outside the spheres, see reference [78] for further discussion.

Our starting point in first principle calculations is that of a parametrized exchange-correlation interaction term in the many-body potential, such as for example the LDA approximation presented in Section (2.4.1), assuming that $E_{xc}[\rho(\mathbf{r})]$ of Equation (2.14) equals that of a homogenous electronic gas. DFT solutions at the LDA level are pursued throughout this chapter, and could equally well have been replaced by any other description of the E_{xc} without loss of generality. This section is to treat the problem of how to implement efficient representations of the wavefunctions in suitable basis sets, $\{\phi_i\}$, in

order to obtain economic solutions[1] to the Kohn-Sham Equations (2.11-2.13) when posed as a numerical eigenvalue problem

$$|\psi\rangle = \sum_{i=i}^{N} c_i |\phi\rangle \tag{3.1}$$

$$(\mathscr{H} - E\mathscr{O})\mathbf{c} = \mathbf{0}, \tag{3.2}$$

with $\{E, \mathbf{c}\}$ the eigensets and

$$\{\mathscr{H}\}_{ij} = \langle \phi_i | H | \phi_j \rangle \tag{3.3}$$

$$\{\mathscr{O}\}_{ij} = \langle \phi_i | \phi_j \rangle, \tag{3.4}$$

the Hamiltonian and overlap matrices respectively. The general task is to solve a standard algebraic eigenvalue problem with a given base *geometry*, regardless of the atomic constituents in the periodic crystal, and to find solutions with smooth transitions between the introduced boundaries. Furthermore, the evaluation of physical properties of crystals requires calculations to be carried out over sample points in the BZ and the integration of periodic functions of Bloch wavevectors, see Section (2.2). Efficient numerical recipes for the sampling of reciprocal space under different symmetries are available in the literature. Standard methods to obtain BZ integrals are special-point schemes [79, 80] and tetrahedron methods [81], both relying on equally spaced grid points inside the BZ.

In the solution of the eigenvalue problem above, one begins with assigning the static background potentials corresponding to each atomic site and then constructing an effective potential V_{eff} in the crystal. The self consistent cycle is started and for each iteration that is performed, the electron density profile is constructed and updated through the Kohn-Sham Equations. A first self-consistent algorithm was presented for the *Hartree-Fock* system of equations in reference [82]. The self-consistent cycle proceeds by improving an initial guess, assuming for instance an electron density distribution as that of isolated atoms, and iterating towards convergence. Because of the orbitals obtained with converged Hartree (H), Hartree-Fock (HF), LDA, and GWA results progress in accuracy with respect to a true solution, these can be used as initial guesses to the more sophisticated models [83] as,

$$H \longrightarrow HF \longrightarrow LDA \longrightarrow GW. \tag{3.5}$$

[1]Economic solutions are achieved when the expansion of the wavefunctions is detailed over regions significant for the formation of bonding states and sparse over the remaining regions.

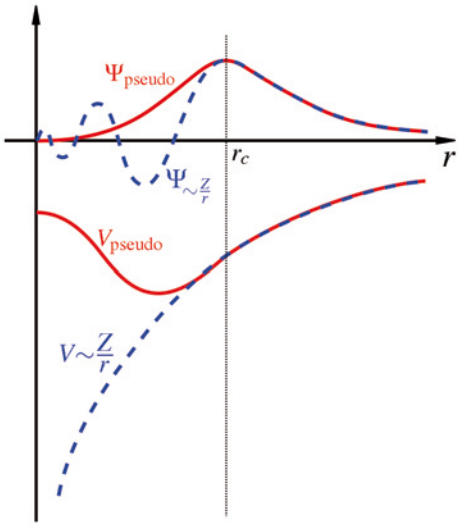

Figure 3.1: Illustration of the pseudo-potential method. In the static Coulomb potential of the nucleus, $V \sim \frac{Z}{r}$ (full line), the pseudo-potential, V_{pseudo} (dashed line), is introduced so that the corresponding wavefunction, $\Psi_{\sim\frac{Z}{r}}$, pseudo-wavefunction, Ψ_{pseudo}, and potentials match at distances larger than a predefined cutoff radius, r_c.

3.1.1 The pseudo-potential method

The most popular among semi-empirical techniques is based on the concept of *pseudo-potentials*, in where the semi-empirical parameters were replaced by self consistent versions, which enabled the calculation of structural and mechanical properties from first principles. The full Coulomb potential includes effects of core electrons and of its nucleus which are substituted by a pseudo-potential [84], so that the Schrödinger equation instead contains a modified effective potential term. In the construction of a pseudo-potential, the valence wavefunction generated can be guaranteed orthogonality to all core states. Such a construct replaces the all-electron potential so that the core states, inert in chemical bonding, are eliminated in the calculation and the valence states are described by pseudo-wavefunctions. Thus, only the chemically active valence electrons are dealt with explicitly. *Norm-conserving* pseudo-potentials are derived from an atomic reference state, requiring that the pseudo- and all-electron valence eigenstates have the same energies and amplitude outside a chosen core cutoff radius r_c. Pseudo-potentials with shorter r_c are said to be softer, and are more efficient with respect to convergence, but at the same time less *transferable*, that is, less accurate in the reproduction of realistic features in different environments, see *Figure 3.1* for an illustration.

Figure 3.2: Illustration of the base geometry of the LMTO method, applicable to an arbitrary crystal. Each element in the crystal i associated with a Muffin-Tin site and with a spherical radius, R_{MT}.

3.1.2 The Linear Muffin-Tin Orbital method

Detailed descriptions of the Linear Muffin-Tin Orbital method [85] (LMTO) can be found in the literature, for example in references [86, 87], here only a brief description will be given emphasizing that the wavefunctions solving the Hamiltonian are expanded in two different regions in space, which are given by a characteristic spherical radius at each atomic site. Inside the centered non-overlapping *Muffin-Tin* region the equations are solved using a potential similar to that of the free atom and the solutions are separated in a radial and an angular contribution. In the remaining *interstitial* region the equations are solved using a constant potential and the basis functions are Neuman or Hankel functions expanded in a Fourier series, see *Figure 3.2* for an illustration of the base geometry employed.

3.1.3 Tight Binding method

In reference [88], Slater and Koster considered the reformulation of the Hamiltonian into a *Tight Binding* (TB) formalism, introducing fitting parameters to reproduce a correct band structure, as

$$H_{\mathrm{TB}} = \sum_{i\nu} \varepsilon_{i\nu} n_{i\nu} + \sum_{\substack{ij\nu\vartheta \\ i\neq j}} t_{ij}^{\nu\vartheta} c_{i\nu}^{\dagger} c_{j\vartheta}, \tag{3.6}$$

in where $n_{i\nu}$ are the occupation numbers for orbital ν of atom i, $t_{ij}^{\nu\vartheta}$ the hopping matrix elements in between created and annihilated orbitals, $c_{i\nu}^{\dagger}$ and $c_{j\vartheta}$ respectively. The $t_{ij}^{\nu\vartheta}$ are used for the interpolation between accurate energy levels at selected $\mathbf{k}$ points that are taken from experimental data or from first principle results. The dimension of H_{TB} reduces to include only a few selected orbitals and the method is thus computationally much more efficient. An extension to TB modeling, in where the required parameters were modified to

be transferable with respect to structural changes of covalent bonded carbon and silicon based materials was presented in references [89, 90, 91, 92].

3.1.4 Calculations within the GW approximation

A similar eigenvalue problem can be posed for the many-body equation within the GW Approximation described in section (2.5.3), where the self energy replaces the LDA exchange-correlation potential in the Hamiltonian. The GW Approximation is usually formulated as a perturbation theory starting from a non-interacting Green's function

$$G^0(\mathbf{k},\omega) = \frac{1}{\omega - H^0_{\mathbf{k}} \pm i\eta}, \tag{3.7}$$

to a given one-body Hamiltonian H^0 as from Equations (2.1-2.2), and η an infinitesimal positive number. Assuming a self-consistent result has been reached, for instance at the LDA level of DFT, the quasiparticle energies are usually constructed from the set of equations,

$$P = -iG^0G^0 \tag{3.8}$$
$$\varepsilon = 1 - V_H P \tag{3.9}$$
$$W^0 = \varepsilon^{-1} V_H \tag{3.10}$$
$$\Sigma = -iG^0W^0, \tag{3.11}$$

The one-body effective Hamiltonian,

$$H(E_k) = -\frac{\nabla^2}{2} + V_{ext} + V_H + \Sigma(E_k), \tag{3.12}$$

is constructed yielding results approximated as a perturbation correction to the LDA from the matrix elements of the diagonal parts of $\Sigma - V_{xc}^{LDA}$ as

$$E^{qp} = E^{LDA} + Z\left[\Sigma(E^{LDA}) - V_{xc}\right], \tag{3.13}$$

where Z is a renormalization factor taking into account that the energy dependence of the self-energy is on E^{LDA} rather than E^{qp}. Since the above formulation depends on the *LDA* it generates reasonable results under limited circumstances where the LDA itself is already a good approximation[2], although the quasiparticle energies computed from the GW Approximation are in better agreement with experiments and also provide information on an excited states lifetime.

[2]For a one-iteration GW scheme to work efficiently, the starting guess solution should be as close as possible to the quasiparticle one.

GW implementations can be classified with respect to the basis geometry employed to describe the wavefunctions and in approximations in calculating the dielectric response, see reference [93] for a review. In particular, when working with a plasmon pole description of ε, as in the model described in reference [94], a frequency close to that of the classical plasma frequency of a homogeneous electron gas at a corresponding electron density is used for the evaluation of Σ, and sets the upper limit for the energy range in where results are accurate. In more sophisticated models [95, 96], one performs a numerical frequency convolution throughout complex plane explicitly. In practice, extending all the functions of frequency to the full complex plane.

3.2 Electron transport with statistical approaches

3.2.1 Monte Carlo and Molecular Dynamics

In Monte Carlo (MC) and Molecular Dynamics (MD) electron transport simulations, Newtons classic equations of motion are used to describe the scattering dynamics, provided accurate quantum mechanical cross sections are available. In the simulation, one has to solve the separate equations of motion for each particle, and follow all particle trajectories and their mutual interaction as well as the interactions with external fields. In each scattering event a single history is estimated from the cross sections. One uses numerical methods to generate probability distributions for all possible events and selects a single event through comparison with random numbers. As the system is evolved in time, a random history of events that emulates the stochastic nature of the process is achieved. The position and velocities of each particle are updated at each time step and simulations of single events are repeated over many times. Physical observables are estimated by averaging results from a large collection of single event histories, these estimates are thus biased with statistical errors. High computational costs which scale with the number of particles restrict the applicability of the MC method to samples of small or moderate sizes. The starting point for the evolution is the excitation of a crystal through interactions with either a photon or an electron. An underlying assumption in the particle transport simulations is that the chain of events is well described as a *Markov* process, that is, that the likelihood of future states at any given moment depends only on its present state and not on its history.

3.2.2 Boltzmann transport theory

The evolution of an energetic particle in a crystal is formally given by the Boltzmann transport equation, which for a given particle density in a phase

space volume element, $d\mathbf{r}d\mathbf{v}$, and at a given time, t, reads

$$\partial_t \rho(\mathbf{r},\mathbf{v},t) + \mathbf{v}\cdot\partial_{\mathbf{r}}\rho(\mathbf{r},\mathbf{v},t) + \frac{\mathbf{F}(\mathbf{r},t)}{m}\cdot\partial_{\mathbf{v}}\rho(\mathbf{r},\mathbf{v},t) = \Omega_{coll}(\rho;\mathbf{r},\mathbf{v},t), \quad (3.14)$$

where $\mathbf{F}(\mathbf{r},t)$ corresponds to the electromagnetic forces acting in the system and $\Omega_{coll}(\rho;\mathbf{r},\mathbf{v},t)$ to a collision operator describing changes in $\rho(\mathbf{r},\mathbf{v},t)$ due to scattering or other short range processes occurring in the system. In a more compact form, the single particle *Liouville* equation is given as [20]

$$i\hbar\frac{\partial\rho}{\partial t} = [H,\rho] \quad (3.15)$$

The Liouville equation reduces to the collisionless Vlasov equation in case of an uncorrelated system. The *Fokker-Planck* equation can be derived as a limiting form of the Liouville equation for long-range forces. A correct description of many-body Coulomb interactions, as that obtained with Fokker-Planck equations can also be obtained with the two-body $\Omega_{coll}(\rho;\mathbf{r},\mathbf{v},t)$ term, assuming Debye cutoff in the Rutherford scattering cross-section [97]. This simplification does not apply to the electron–electron interactions, where the charged particles in the scattering have identical charges, and the momentum transfer during their collision cannot be neglected [98]. Computational schemes for the numerical solutions of the Euler, Rugne-Kutta and higher order adaptive methods are available in the literature, see for instance reference [99].

4. Results

In this chapter an overview of results presented in *Papers I-V* is given.

4.1 Data mining and accelerated electronic structure theory as a tool in the search for new functional materials

Scintillators are widely used as radiation detectors, for example, in the life sciences. In Positron Emission Tomography (PET) a short-lived radioactive tracer isotope generates a signal at a region of interest, for example, a fluorodeoxyglucose (FDG) sugar molecule containing an ^{18}F isotope of roughly 2 hours half-life finding its way to a tumor region of high metabolism. As the isotope decays, it emits positrons through β-decay which, being anti-matter, annihilate when interacting with the medium and emit two collinear or back-to-back photons at energies equal to the electron rest mass, 511 keV. Inorganic scintillator crystals are preferred in applications where high photon stopping power is required, as their density and effective atomic number can be much larger than that of organic scintillators. Many of the inorganic scintillating materials have also very high light output and can provide good energy resolution down to very low energies. Some materials are intrinsic scintillators, whereas other require the addition of a dopant, typically fluorescent ions such as Ce. In complex crystals, the temporal resolution of the scintillating process is given by the rate at which the radiative processes occurs in the luminescent center, which is of the order of a few tens of nanoseconds in Ce-doped materials and one to two orders of magnitude higher in Tl-doped materials. The detection of two collinear photons represents a line in space, connecting the two detectors along the direction of the emission. As photons travel at a speed of about 30 cm ns^{-1}, a temporal resolution in the sub-nanosecond range is needed to resolve the origin of the annihilation process spatially, such systems are refereed to in the literature as Time-Of-Flight PET (TOF-PET).

In *Paper I*, a highly accelerated electronic structure implementation and data mining algorithms have been combined with structural data from the Inorganic Crystal Structure Database to generate materials properties for about 22,000 inorganic compounds. It is shown how data mining algorithms employed on the database can identify new functional materials with desired

materials properties. A study is presented in the case of crystals with potential for use as scintillator detector materials, resulting in a prediction of 136 novel candidates. The methodology behind the automatized first principle approach is presented and the selection rules applied to the database are motivated from both macroscopic material properties and quantum mechanical electronic structure properties. Electronic structure results are tabulated and a version of the complete database is made available at the internet web site `http://gurka.fysik.uu.se/ESP`.

4.2 Secondary electron cascade dynamics in KI and CsI

High resolution in the detection of photons involves generally the production of an electrical signal from a very small number of incident photons. The electrical signal extracted from a material has its origin in three different processes, (i) the generation of primary photoelectrons or electron–hole (e-h) pairs by the incident photons, (ii) production of secondary electron (SE) cascades or avalanches through non-radiative decays, and (iii) the extraction and detection of SEs. Ultra-fast phenomena are typically studied using pump–probe techniques where the dynamics are initiated by a pump laser and probed using X-rays after some time delay. If pulses from different sources are used, time jittering between the pump and the probe will limit the temporal resolution of the measurement, so an accurate synchronization between the two is of primary concern. In alternative experimental setups where the same pulse is used as both pump and probe, as in holography experiments, time jittering is not an issue.

Streak cameras can be used to characterize spatio–temporal features of a light source. Optoelectronic streak cameras work by directing light onto a photocathode, whereby ionization through the photoelectric effect takes place. As the released photo-electrons evolve in the sample, secondary ionization is promoted through non-radiative relaxation processes and an electron yield is achieved in the cathode material. Electrons leaving the cathode material are accelerated in a cathode ray tube and projected into an anode. Their distribution in energy carries valuable information and in their passage trough the ray tube an electric field deflecting their trajectories is applied. By quick changes in the electric field the deflection is modulated and a streak image obtained in where control is gained over the electron's arrival at the anode. A linear detector, such as a charge-coupled device array is used to measure the streak pattern on the anode. Every point in a streak image provides thus information representing intensity, location, and time, from which the pulse's spatio–temporal characteristics are determined. The streak camera's resolution and efficiency is determined

by the electron yield of the cathode material and the SEs distribution in energy.

In *Paper II*, we combine an existing model for the generation secondary electron cascade dynamics, following an Auger relaxation process in the photocathode material, with both experimental and first principle results for the dielectric response function, $\varepsilon(\mathbf{q}, \omega)$, the latter often absent in the literature. One aim, is to study the stability of the cascade model with respect to a calculated energy loss function at the optical limit, -Im $\varepsilon^{-1}(0, \omega)$. A second aim, is to compare the secondary electron cascade dynamics in two different photocathode materials, namely KI and CsI. A comparison between the electron yield and the SEs energy distributions in each material is given. Our results show comparable saturation times and secondary electron yields for the cascades in the two materials, and a narrower electron distribution (51%) for KI compared with CsI.

4.3 Radiation damage in biological material: Electronic properties and electron impact ionization in urea and

X-ray Free Electron Lasers techniques will deliver ultra-short pulses of unprecedented intensities in the near future. The realization of single bioparticle imaging is one of the goals to be pursued at such facilities. Radiation damage is an unavoidable process when performing structural investigations of biological macromolecules with X-rays, and a major issue in the recording of a diffraction pattern in imaging experiments as the sample becomes excited by the pulse and structural changes, or damage to the original structure, follows. In crystallography this process can be limited through damage distribution in a crystal, while for single molecular imaging it can be outrun by employing short intense pulses.

On a time scale longer than 5 fs, most of the ionizations in a sample exposed to an X-ray pulse will not be due to primary photo ionizations, but due to inelastic electron scattering. In the aftermath of a single photo ionization, the photo electron as well as consecutive Auger electrons will interact with outer shell electrons in the surrounding atoms, leading to an electron cascade. This process is exploited when detecting photons in photo-multipliers, but leads to undesired ionization and structure damage in diffractive imaging.

In *Paper III*, a theoretical study of secondary electron cascades in a small biological crystal is presented. Secondary electron generation is crucial during damage formation and we perform a study on the spatio–temporal characteristics of the SE cascade for urea $CO(NH_2)_2$. Urea bears more similarities with the biological matter in both elemental composition and density, making

it a more suitable object of theoretical study than for example water or diamond, especially when addressing large systems. Cross sections are derived from first principle calculations, furthermore, we describe the size of the electron cloud generated through impact ionization as a function of the electron energy, showing the spatial extent of the radiation damage due to secondary ionization.

4.4 Nanocrystal imaging using intense and ultrashort X-ray pulses

Any sample exposed to an intense X-ray pulse will be ionized, and extensive ionization destroys the sample. The time scale on which this process occurs is critical for obtaining an interpretable diffraction pattern to yield an atomic structure of the sample. In principle, the X-ray pulse must be short enough such that the diffraction pattern is recorded before major reconfigurations in the electron population and the atomic positions takes place.

Ionizations due to the direct photoabsorption and subsequent secondary processes affect the ability to get useful structural information from the diffraction pattern in three ways. (i) Ionization decreases the elastic X-ray scattering power of the atoms. (ii) Removal of electrons from the atoms leaves behind positively charged ions that repel each other due to Coulomb forces, leading to the destruction of the structure. (iii) Free electrons either leave the sample, if their energy is high enough, or remain in the sample as an excited background electron gas, in which case they will contribute to noise in the diffraction pattern.

In *Paper IV*, we address the potentials and limitations of nanocrystallography with extremely intense coherent X-ray pulses. We use results of *Paper III* for urea nanocrystals as a model for generic biological substances, and simulate the primary and secondary ionization dynamics in the crystalline sample. The results establish conditions for diffraction experiments as a function of X-ray fluence, pulse duration, and the size of nanocrystals.

4.5 Radiation damage in covalent solids by intense ultra-short soft X-ray pulses

Carbon based materials are used in the transport of the pulse at XFEL facilities, and are being considered for the European XFEL project. A poor understanding of the damage induced through intense irradiation represents

a severe limitation in the design of optical elements. Through irradiation with intense femtosecond soft X-ray pulses the structural damage originating from ultra-fast non-thermal phase transitions is observed. A computational model which combines electronic structure theory with molecular dynamics (MD) for the atomic motion is extended to include interactions relevant at soft X-ray wavelengths (6-13.5 nm). Dedicated Boltzmann transport equation is derived, with electron relaxation rates calculated from density functional theory and energy loss function from binary encounter theory. Preliminary results for diamond are presented and compared to the earlier predictions from Molecular Dynamics (MD) simulations.

In *Paper V*, first principle results for the relaxation rates of excited states of diamond are derived from first principles. Impact ionization is implemented through a dedicated Boltzmann transport equation using first principle results for the relaxation rates and Binary-Encounter results for the derivation of cross sections. Preliminary results are presented for the implementation of the Boltzmann Transport equation using an Euler integration method. The treatment of plasmon decay is also available from first principles.

5. Svensk sammanfattning

Hade den här avhandlingen skrivits för 100 år sedan hade den varit nära besläktad med dåvarande forskning på fotografiska kameror, och möjligen behandlat frågor som: Vilka egenskaper bör en filmrulle ha för att fånga ljuset som registreras under tiden slutaren är öppen? Fenomenet som ger upphov till ett avtryck på en filmrulle, den fotoelektriska effekten eller elektronernas absorption av energin som bärs av ljuskvanta eller fotoner, är fortfarande aktuellt här, men istället handlar min avhandling om hur materialegenskaper härledda från kvantmekaniska beräkningar kan användas i andra applikationer, där man försöker utvinna information som bärs av enskilda eller väldigt få fotoner, och där avbildningsobjekten kräver en upplösning på atomär nivå. Materialen som studeras faller inom kategorin *kondenserad materia*, med det menas att materialen är fasta och har en stabil struktur, exempelvis kisel atomer i en kristall som används i elektroniska kretsar. Kristallstrukturen uppkommer och hålls ihop av bindningar som har sin ursprung i elektromagnetisk växelverkan av de elektrisk laddade elektronerna. Elektronstrukturen i en kristall är unik och de tillåtna tillstånden för elektronens rörelse, eller orbitaler, beskriver bindningarna. Materialegenskaper är beroende av elektronstrukturens tillåtna tillstånd, och vid en energi nära bindningstillståndens måste en detaljerad kvantmekanisk beskrivning ingå, se *Figur 5.1*. Vid en mycket högre energi är elektronrörelsen väsentligen fri från bindningarna i kristallen. Delvis handlar denna avhandling också om en ny generation av ljuskällor, Fri Elektron Lasern, som nu gör sitt inträde i den vetenskapliga världen. Dessa källor ger upphov till ljuspulser med intensiteter i storleksordningen miljard gånger större än konventionella källor. Förväntningarna är att foton tillgängligheten kommer att möjliggöra nya typer observationer, av vilka två typer behandlas i de två sista artiklarna.

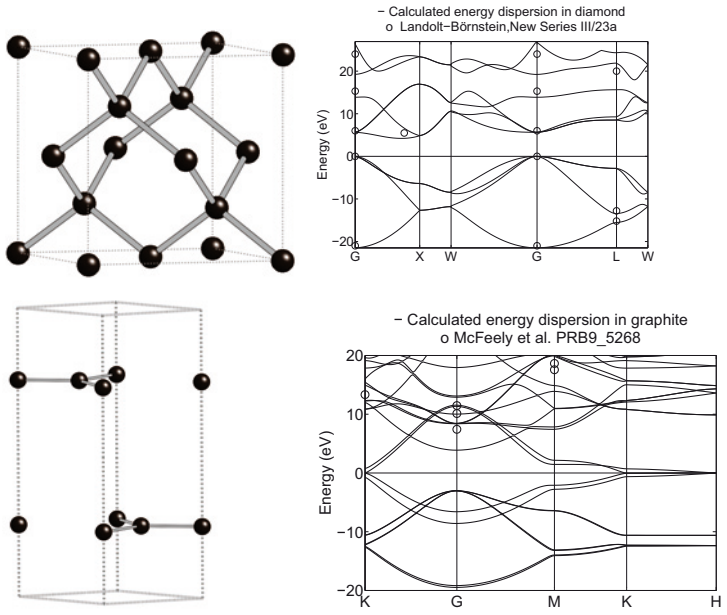

Figure 5.1: Kristallstruktur och bandstruktur hos diamant (ovan) och grafit (nedan).

Fem artiklar presenteras.

Artikel I Behandlar konstruktionen av en stor databas med information om elektronstrukturegenskaper hos en stor samling kristaller med känd kristall struktur. Databasstudier är lämpliga vid sökning av nya kandidatmaterial vars funktionalitet kan associeras till egenskaper härstammande från elektronstrukturen. En exempelstudie presenteras för scintilatorer, lämpliga för avbildning av vävnader inom medicinsk teknik.

Artikel II Behandlar signalen som utvinns ur en fotokatod i så kallade *streak* kameror, lämpliga vid studier av en strålkällas intensitetsvariation i rum och tid.

Artikel III Behandlar elekronkaskadsprocesser i urea, bättre lämpad vid studier av strålningsskador inom strukturell biofysik än till exempel vatten eller diamant då den innehåller biologins väsentliga komponenter, kol, väte, syre, och kväve.

Artikel IV Behandlar tidsaspekten på skador uppkomna under avbildningen av en biologisk molekyl genom Fri Elektron Laser (XFEL) bestrålning och använder sig delvis av resultaten från artikel IV.

Artikel V Behandlar strukturskador uppkomna på ytor av kol-kristaller, ett kovalent bundet material, efter intensiv Fri Elektron Laser bestrålning. Kolbaserade material används för pulstransport i XFEL anläggningar, se *Figur 5.2*.

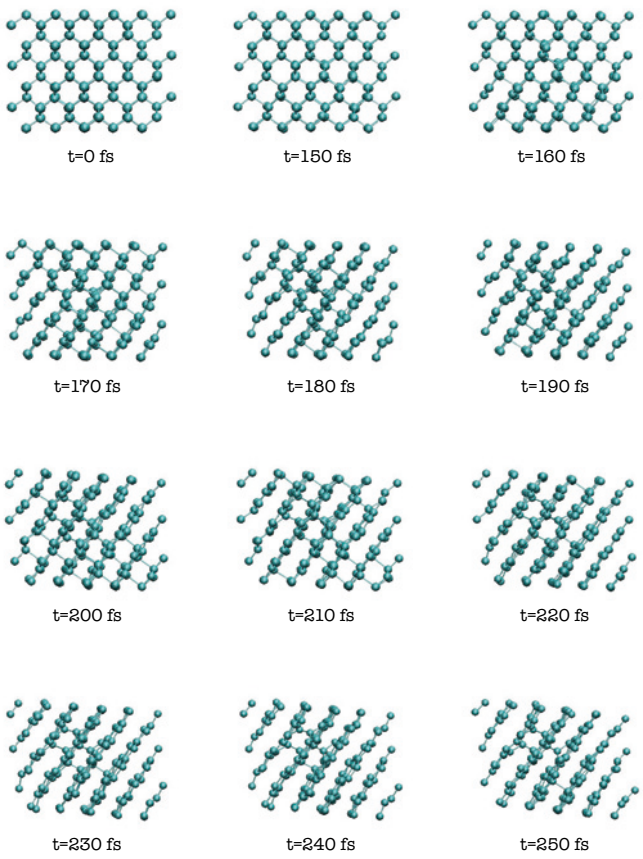

Figure 5.2: Bild av simulerad strukturförändring i diamant.

6. Acknowledgments

Picture yourself entering a room where a 3000 year old conversation is taking place. The discussion is about what we now days call physics, thus the people inside the room talk about different aspects of matter. What it is, how it interacts, how we perceive it and how we might take advantage of it. Your task, entering the room as a PhD student, is to form yourself with an opinion regarding a few selected topics and deliver timely comments expressing your point of view. During this process you gain much insight into different aspects of research and why you might engage in such an activity. Choosing a topic and gathering information before reporting my opinion was not an easy task for me, and I have received invaluable help from many people. I am thankful to my supervisors Mattias Klintenberg and Olle Eriksson for giving me the opportunity to do what i now present here and for providing the stimulating environment in which it took place. I am also thankful to Beata Ziaja-Motyka for her invitation to Hamburg and for showing me how theoretical modeling is done from a ninja's perspective.

I also want to acknowledge the support from colleges whom i owe special thanks: Anders Bergman, Andreas Blomqvist, Andreas Höglund, Anton Grigoriev, Anna Delin,, Biplab Sanyal, Björn Skubic, Börje Johansson, Carl Caleman, Cecilia Århammar, Daniel Åberg, Diana Iusan, Dominik Legut, Elisabeth Bill, Erik Marklund, Francesco Cricchio, Fredrik Bultmark, Fredrik Silvervarv, Giorgio Favrin, Gunnel Ingelög, Gösta Huldt, Haroula Rouki, Ingmar Sandberg, Jailton Almieda, Jan Rusz, Janos Hajdu, Jarl Nissfolk, Jérôme Gaudin, Johan Hellsvik, Jonas Fransson, Kim Duck-Young, Klas Andersson, Lars Bergqvist, Lars Nordström, Love Kocî, Magnus Bergh, Markus Gabrysch, Martin Amft, Matthew Darmalingum, Michi-To Suzuki, Mikael Råsander, Moyses Araujo, Mårten Stenmark, Nicuşor Tîmneanu, Niklas Ottoson, Ola Wessely, Oleg Peil, Oscar Grånäs, Peter Larsson, Peter Oppeneer, Petros Souvatzis, Rajeev Ahuja, Ralph Scheicher, Sebastien Lebegue, Sergiu Arapan, Stefan Plogmaker, Susanne Mirbt, Thomas Dziekan, Till Burkert, Torbjörn Björkman, Velimir Meded, Wei Luo, Weine Olovsson, Younsuk Yun. To Vendela, my family, and the rest of my tribe, I want to express my love and gratitude.

Bibliography

[1] B. H. Bransden and C. J. Joachain. Physics of Atoms and Molecules. Longman Group Limited, 1983.

[2] N. Ashcroft and N. Mermin. Solid State Physics. Thomson Learning, 1976.

[3] K. Capelle. A bird's-eye view of density-functional theory. *arXiv:cond-mat/0211443*.

[4] R. Jones and O. Gunnarsson. The density functional formalism, its applications and prospects. *Rev. Mod. Phys*, 61:689, 1989.

[5] D. Pines. Elementary Excitations in Solids. *Advanced book classics*. Reading, Mass. : Perseus, 1999.

[6] G. D. Mahan. Many-Particle Physics. Kluwer Academics / Plenum Publishers, 2000.

[7] A. Georges. Strongly correlated electron materials: Dynamical mean-field theory and electronic structure. *AIP Conf. Proc.*, 715:3, 2004. *Arxiv:cond-mat/0403123*.

[8] M. Inokuti. Inelastic Collisions of Fast Charged Particles with Atoms and Molecules-The Bethe Theory Revisited. *Rev. Mod. Phys*, 43:297, 1971.

[9] F. Aryasetiawan and O. Gunnarsson. The GW method. *Rep. Prog. Phys*, 61:237, 1998.

[10] L. Hedin. On correlation effects in electron spectroscopies and the GW approximation. *J. Phys.: Condens. Matter*, 11:R489, 1999.

[11] M. Aroyo, A. Kirov, C. Capillas, J. Perez-Mato, and H. Wondratschek. Bilbao Crystallographic Server. II. Representations of crystallographic point groups and space groups *Acta Crystallogr.*, A62:115, 2006.

[12] P. Hohenberg and W. Kohn. Inhomogeneous Electron Gas. *Phys. Rev.*, 136:B864, 1964.

[13] W. Kohn and L. Sham. Self-Consistent Equations Including Exchange and Correlation Effects. *Phys. Rev.*, 140:A1133, 1965.

[14] W. Hanke and L. Sham. Local-field and excitonic effects in the optical spectrum of a covalent crystal. *Phys. Rev. B*, 12:4501, 1975.

[15] D. Ceperley and B. Alder. Ground State of the Electron Gas by a Stochastic Method. *Phys. Rev. Lett.*, 45:566, 1980.

[16] J. Perdew and A. Zunger. Self-interaction correction to density-functional approximations for many-electron systems. *Phys. Rev. B*, 23:5048, 1981.

[17] C. O. Almbladh and U. von Barth. Exact results for the charge and spin densities, exchange-correlation potentials, and density-functional eigenvalues. *Phys. Rev. B*, 31:3231, 1985.

[18] W. Kohn. Nobel lecture: Electronic structure of matter–wave functions and density functionals. *Rev. Mod. Phys.*, 71:1253, 1999.

[19] O. Gunnarsson and B. Lundqvist. Exchange and correlation in atoms, molecules, and solids by the spin-density-functional formalism. *Phys. Rev. B*, 13:4274, 1976.

[20] H. Ehrenreich and M. Cohen. Self-Consistent Field Approach to the Many-Electron Problem. *Phys. Rev.*, 115:786, 1959.

[21] D. Pines and D. Bohm. A Collective Description of Electron Interactions: II. Collective vs Individual Particle Aspects of the Interactions. *Phys. Rev.*, 85:338, 1952.

[22] J. J. Quinn. Range of Excited Electrons in Metals. *Phys. Rev.*, 126:1453, 1962.

[23] J. Lindhard. On the properties of a gas of charged particles. *K. Dan. Vidensk. Selsk. Mat. Fys. Medd.*, 28:1, 1954.

[24] P. Nozières and D. Pines. Electron Interaction in Solids. Characteristic Energy Loss Spectrum. *Phys. Rev.*, 113:1254, 1959.

[25] S. Adler. Quantum Theory of the Dielectric Constant in Real Solids. *Phys. Rev.*, 126:413, 1962.

[26] N. Wiser. Dielectric Constant with Local Field Effects Included. *Phys. Rev.*, 129:62, 1963.

[27] M. Altarelli, D. Dexter, H. Nussenzveig, and D. Smith. Superconvergence and Sum Rules for the Optical Constants. *Phys. Rev. B*, 6:4502, 1972.

[28] M. Altarelli and D. Smith. Superconvergence and sum rules for the optical constants: Physical meaning, comparison with experiment, and generalization. *Phys. Rev. B*, 9:1290, 1974.

[29] B. Lundqvist. Some Numerical Results on Quasiparticle Properties in the Electron Gas. *Phys. Status Solidi*, 32:273, 1969.

[30] Philippe Nozières and David Pines. Electron Interaction in Solids. General Formulation. *Phys. Rev.*, 109:741, 1958.

[31] L. Hedin. New Method for Calculating the One-Particle Green's Function with Application to the Electron-Gas Problem. *Phys. Rev.*, 139:A796, 1965.

[32] M. van Schilfgaarde, T. Kotani, and S. Faleev. Quasiparticle Self-Consistent GW Theory. *Phys. Rev. Lett.*, 96:226402, 2006.

[33] G. Onida, L. Reining, and A. Rubio. Electronic excitations: density-functional versus many-body Green's-function approaches. *Rev. Mod. Phys.*, 74:601, 2002.

[34] C. Amsler, et. al. Review of Particle Physics. *Phys. Lett. B*, 667:1, 2008.

[35] J. H. Hubbell, Wm. J. Veigele, E. A. Briggs, R. T. Brown, D. T. Cromer, and R. J. Howerton. Atomic form factors, incoherent scattering functions, and photon scattering cross sections. *J. Phys. Chem. Ref. Data*, 4:471, 1975.

[36] A. Haug, D. Kerkhoff, and W. Lochmann. Calculation of Auger Coefficients for III-V Semiconductors with Emphasis on GaSb. *Phys. Status Solidi B*, 89:357, 1978.

[37] D. Laks, G. Neumark, and S. Pantelides. Accurate interband-auger-recombination rates in silicon. *Phys. Rev. B*, 42:5176, 1990.

[38] Y. Shen, G. Mueller, S. Watanabe, N. Gardner, A. Munkholm, and M. Krames. Auger recombination in InGaN measured by photoluminescence. *Appl. Phys. Lett.*, 91:141101, 2007.

[39] V. Ayvazyan, et al. First operation of a free-electron laser generating GW power radiation at 32 nm wavelength. *Eur. Phys. J. D*, 37(2):297, 2006.

[40] L. DiMauro, J. Arthur, N. Berrah, J. Bozek, J. Galayda, and J. Hastings. Progress report on the LCLS XFEL at SLAC. *J. Phys.: Conf. Ser.*, 88:012058, 2007.

[41] T. Shintake, et al. A compact free-electron laser for generating coherent radiation in the extreme ultraviolet region. *Nat. Photon.*, 2:555, 2008.

[42] M. Altarelli, et al. The Technical Design Report of the European XFEL (DESY 2006-097). `http://xfel.desy.de/tdr/tdr/`.

[43] K. Gaffney and H. Chapman. Imaging Atomic Structure and Dynamics with Ultrafast X-ray Scattering. *Science*, 316:1444, 2007.

[44] R. Neutze, R. Wouts, D. van der Spoel, E. Weckert, and J. Hajdu. Potential for biomolecular imaging with femtosecond X-ray pulses. *Nature*, 406:752, 2000.

[45] J. Hajdu. Single-molecule X-ray diffraction. *Curr. Opin. Struct. Biol.*, 10:569, 2000.

[46] B. Ziaja, H. Wabnitz, E. Weckert, and T. Möller. Atomic clusters of various sizes irradiated with short intense pulses of VUV radiation. *EPL (Europhys. Lett.)*, 82, 2008.

[47] S. P. Hau-Riege, R. A. London, and A. Szoke. Dynamics of biological molecules irradiated by short x-ray pulses. *Phys. Rev. E*, 69:051906, 2004.

[48] Z. Jurek, G. Faigel, and M. Tegze. Dynamics in a cluster under the influence of intense femtosecond hard X-ray pulses. *Eur. Phys. J. D*, 29:217, 2004.

[49] M. Bergh, N. Tîmneanu, and D. van der Spoel. Model for the dynamics of a water cluster in an x-ray free electron laser beam. *Phys. Rev. E*, 70(5):051904, Nov 2004.

[50] A. Barbieri and M. A. Van Hove. Private communication, `http://www.ap.cityu.edu.hk/personal-website/Van-Hove.htm`.

[51] N. Bohr. Theory of the decrease of velocity of moving electrified particles on passing through matter. *Philos. Mag. (1798-1977)*, 25:10, 1913.

[52] H. Bethe. Zur theorie des durchgangs schneller korpuskularstrahlen durch materie. *Ann. Phys. (Leipzig)*, 5:325, 1930.

[53] U. Fano. Penetration of Protons, Alpha Particles, and Mesons. *Annu. Rev. Nucl. Sci.*, 13:1, 1963.

[54] R. Ritchie. Interaction of Charged Particles with a Degenerate Fermi-Dirac Electron Gas. *Phys. Rev.*, 114:644, 1959.

[55] C. J. Powell. Attenuation lengths of low-energy electrons in solids. *Surf. Sci.*, 44:29, 1974.

[56] D. Penn. Electron Mean Free Paths for Free-electron-like Materials. *Phys. Rev. B*, 13:5248, 1976.

[57] S. Tanuma, C. J. Powell, and D. R. Penn. Calculations of Electron Inelastic Mean Free Paths for 31 Materials. *Surf. Interface Anal.*, 11:577, 1988.

[58] S. Tanuma, C. J. Powell, and D. R. Penn. Calculations of Electorn Inelastic Mean Free Paths. II. Data for 27 elements over the 50-2000 eV range. *Surf. Interface Anal.*, 17:911, 1991.

[59] S. Tanuma, C.J. Powell, and D.R. Penn. Calculations of Electron Inelastic Mean Free Paths. V. Data for 14 Organic Compounds over the 50-2000 eV Range. *Surf. Interface Anal.*, 21:165, 1994.

[60] J. Ashley. Interaction of low-energy electrons with condensed matter: Stopping powers and inelastic mean free paths from optical data. *J. Electron Spectrosc. Relat. Phenom.*, 46:199, 1988.

[61] N. F. Mott. The Collision between Two Electrons. *Proc. R. Soc. London Ser. A*, 126:259, 1930.

[62] Y. Kim and M. E. Rudd. Binary-encounter-dipole model for electron-impact ionization. *Phys. Rev. A*, 50:3954, 1994.

[63] E. O. Kane. Need for a Nonlocal Correlation Potential in Silicon. *Phys. Rev. B*, 4:1910, 1971.

[64] E. O. Kane. Electron Scattering by Pair Production in Silicon. *Phys. Rev.*, 159:624, 1967.

[65] E. O. Kane. Simple Model for Collision Effects in Photoemission. *Phys. Rev.*, 147:335, 1966.

[66] B. L. Henke, J. Liesegang, and S. D. Smith. Soft-x-ray-induced secondary-electron emission from semiconductors and insulators: Models and measurements. *Phys. Rev. B*, 19:3004, 1979.

[67] G. W. Fraser. The characterisation of soft x-ray photocathodes in the wavelength band 1-300 Å: II. Caesium iodide and other insulators of high photoelectric yield. *Nucl. Instr. Methods*, 206:265, 1983.

[68] G. W. Fraser. The characterisation of soft X-ray photocathodes in the wavelength band 1-300 Å: I. Lead glass, lithium fluoride and magnesium fluoride *Nucl. Instr. Methods*, 206:251, 1983.

[69] A. Akkerman, T. Boutboul, A. Breskin, R. Chechik, and A. Gibrekhterman. Low-energy electron transport in alkali halides. *J. Appl. Phys.*, 76:4656, 1994.

[70] A. Akkerman, A. Gibrekhterman, A. Breskin, and R. Chechik. Monte carlo simulations of secondary electron emission from CsI, induced by 1–10 keV x rays and electrons. *J. Appl. Phys.*, 72:5429, 1992.

[71] A. Akkerman and E. Akkerman. Characteristics of electron inelastic interactions in organic compounds and water over the energy range 20–10 000 eV. *J. Appl. Phys.*, 86:5809, 1999.

[72] T. Boutboul, A. Akkerman, A. Breskin, and R. Chechik. Escape length of ultraviolet induced photoelectrons in alkali iodide and CsBr evaporated films: Measurements and modeling. *J. Appl. Phys.*, 84:2890, 1998.

[73] T. Boutboul, A. Akkerman, A. Breskin, and R. Chechik. Electron inelastic mean free path and stopping power modelling in alkali halides in the 50 eV–10 keV energy range. *J. Appl. Phys.*, 79:6714, Jan 1996.

[74] A. Akkerman, T. Boutboul, A. Breskin, and R. Chechik. Inelastic electron interactions in the energy range 50 eV to 10 keV in insulators: Alkali Halides and Metal Oxides. *Phys. Status Solidi B*, 198:769, 1996.

[75] A. I. Gusarov and S. V. Murashov. The role of the plasmon mechanism in the secondary electron emission in LiF. *Surf. Sci.*, 320:361, 1994.

[76] F. Herman. Theoretical Investigation of the Electronic Energy Band Structure of Solids. *Rev. Mod. Phys*, 30:102, 1958.

[77] FIZ Karlsruhe. ICSD, Inorganic Crystal Structure Database. `http://www.fiz-karlsruhe.de/icsd.html`.

[78] J. Slater. Electronic energy bands in metals. *Phys. Rev.*, 45:794, 1934.

[79] R. Evarestov and V. Smirnov. Special points of the Brillouin zone and their use in the solid state theory. *Phys. Status Solidi B*, 119:9, 1983.

[80] H. Monkhorst and J. Pack. Special points for Brillouin-zone integrations. *Phys. Rev. B*, 13:5188, 1976.

[81] P. Blöchl, O. Jepsen, and O. K. Andersen. Improved tetrahedron method for Brillouin-zone integrations. *Phys. Rev. B*, 49:16223, 1994.

[82] E. Wigner and F. Seitz. On the constitution of metallic sodium. II. *Phys. Rev.*, 46:509, 1934.

[83] L. Hedin. Electron correlation: Keeping close to an orbital description. *Int. J. Quantum Chem.*, 56:445, 1995.

[84] H. Hellmann. A new approximation method in the problem of many electrons. *J. Chem. Phys.*, 3:61, 1935.

[85] J. Slater. Wave functions in a periodic potential. *Phys. Rev.*, 51:846, 1937.

[86] H. L. Skriver. The LMTO Method: Muffin-Tin Orbitals and Electronic Structure. Springer Verlag, 1984.

[87] J. M. Wills, O. Eriksson, M. Alouani, and D. L. Price. Electronic Structure and Physical Properties of Solids: The uses of the LMTO method. Springer Verlag, 2000

[88] J. Slater and G. Koster. Simplified LCAO method for the periodic potential problem. *Phys. Rev.*, 94:1498, 1954.

[89] L. Goodwin, A. Skinner, and D. Pettifor. Generating transferable tight-binding parameters: Application to silicon. *EPL (Europhys. Lett.)*, 9:701, 1989.

[90] C. Xu, C. Wang, C. Chan, and K. Ho. A transferable tight-binding potential for carbon. *J. Phys.: Condens. Matter*, 4:6047, 1992.

[91] I. Kwon, R. Biswas, C. Wang, K. Ho, and C. Soukoulis. Transferable tight-binding models for silicon. *Phys. Rev. B*, 49:7242, 1994.

[92] A. Horsfield, P. Godwin, D. Pettifor, and A. Sutton. Computational materials synthesis. I. A tight-binding scheme for hydrocarbons. *Phys. Rev. B*, 54:15773, 1996.

[93] M. van Schilfgaarde, T. Kotani, and S. Faleev. Adequacy of approximations in GW theory. *Phys. Rev. B*, 74:245125, 2006.

[94] M. Hybertsen and S. Louie. Electron correlation in semiconductors and insulators: Band gaps and quasiparticle energies. *Phys. Rev. B*, 34:5390, 1986.

[95] S. Lebegue, B. Arnaud, M. Alouani, and P. E. Bloechl. Implementation of an all-electron GW approximation based on the projector augmented wave method without plasmon pole approximation: Application to Si, SiC, AlAs, InAs, NaH, and KH *Phys. Rev. B*, 67:155208, 2003.

[96] M van Schilfgaarde, T. Kotani, and S. Faleev. Quasiparticle self-consistent GW theory. *Phys. Rev. Lett.*, 96:226402, 2006.

[97] S. Chapman and T. G. Cowling. *The Mathematical Theory of Non-Uniform Gases.* Cambridge University Press, 1970.

[98] B. Ziaja, E. Weckert, and T. Möller. Statistical model of radiation damage within an atomic cluster irradiated by photons from free-electron-laser. *Laser Part. Beams*, 25:407, 2007.

[99] W. H. Press, S. A. Teukolsky, W. T. Vetterling, and B. P. Flannery. *Numerical Recipes 3rd Edition: The Art of Scientific Computing*. Cambridge University Press, 2003.

Acta Universitatis Upsaliensis

Digital Comprehensive Summaries of Uppsala Dissertations from the Faculty of Science and Technology 652

Editor: The Dean of the Faculty of Science and Technology

A doctoral dissertation from the Faculty of Science and Technology, Uppsala University, is usually a summary of a number of papers. A few copies of the complete dissertation are kept at major Swedish research libraries, while the summary alone is distributed internationally through the series Digital Comprehensive Summaries of Uppsala Dissertations from the Faculty of Science and Technology. (Prior to January, 2005, the series was published under the title "Comprehensive Summaries of Uppsala Dissertations from the Faculty of Science and Technology".)

Distribution: publications.uu.se
urn:nbn:se:uu:diva-102376

ACTA
UNIVERSITATIS
UPSALIENSIS
UPPSALA
2009